Regulation of a Cytochrome P450 Gene *CYP94B1* by WRKY33 Transcription Factor Controls Apoplastic Barrier Formation in Roots to Confer Salt Tolerance[1][OPEN]

Pannaga Krishnamurthy,[a,b] Bhushan Vishal,[a,2] Wan Jing Ho, Felicia Chien Joo Lok, Felicia Si Min Lee,[a] and Prakash P. Kumar[a,b,3,4]

[a]Department of Biological Sciences, National University of Singapore, Singapore 117543
[b]National University of Singapore Environmental Research Institute (NERI), National University of Singapore, Singapore 117411

ORCID IDs: 0000-0002-8483-6731 (P.K.); 0000-0001-7972-4180 (B.V.); 0000-0002-0963-1664 (P.P.K.).

Salinity is an environmental stress that causes decline in crop yield. *Avicennia officinalis* and other mangroves have adaptations such as ultrafiltration at the roots aided by apoplastic cell wall barriers to thrive in saline conditions. We studied a cytochrome P450 gene from *A. officinalis*, *AoCYP94B1*, and its putative ortholog in Arabidopsis (*Arabidopsis thaliana*), *AtCYP94B1*, which are involved in apoplastic barrier formation. Both genes were induced by 30 min of salt treatment in the roots. Heterologous expression of *AoCYP94B1* in the *atcyp94b1* Arabidopsis mutant and wild-type rice (*Oryza sativa*) conferred increased NaCl tolerance to seedlings by enhancing root suberin deposition. Histochemical staining and gas chromatography-tandem mass spectrometry quantification of suberin precursors confirmed the role of CYP94B1 in suberin biosynthesis. Using chromatin immunoprecipitation and yeast one-hybrid and luciferase assays, we identified AtWRKY33 as the upstream regulator of *AtCYP94B1* in Arabidopsis. In addition, *atwrky33* mutants exhibited reduced suberin and salt-sensitive phenotypes, which were rescued by expressing *35S::AtCYP94B1* in the *atwrky33* background. This further confirmed that AtWRKY33-mediated regulation of *AtCYP94B1* is part of the salt tolerance mechanism. Our findings may help efforts aimed at generating salt-tolerant crops.

Salinity is a major environmental stress factor that leads to reduced crop productivity. The progressive increase in soil salinization exacerbates the already damaging effect of steady reduction in the area of arable land worldwide (Parida and Das, 2005; Agarwal et al., 2014). Na^+ is the major toxic ion found in high saline soils, and it imparts osmotic as well as ionic stresses. It is imperative to limit the entry of excess Na^+ into plant cells to maintain proper ion homeostasis and normal metabolism. Mangroves have evolved various adaptive strategies to flourish under high saline conditions. One of the important adaptations exhibited by most plants, and to a greater extent by mangroves, is ultrafiltration at the roots by the presence of apoplastic barriers in the roots (Scholander, 1968). In an earlier study, we showed that a salt secretor mangrove, *Avicennia officinalis*, restricts 90% to 95% salt at the roots due to the presence of enhanced apoplastic barriers (Krishnamurthy et al., 2014).

The main apoplastic diffusion barriers in roots are epidermis, which is the outermost layer of young roots, endodermis surrounding the vasculature of young roots, and peridermis, which replaces both epidermis and endodermis in the older roots upon secondary thickening (Nawrath et al., 2013; Wunderling et al., 2018). These apoplastic barriers mainly consisting of Casparian strips (CSs) and suberin lamellae (SLs) block the apoplastic and coupled transcellular leakage of ions and water into the xylem, which is the major path of Na^+ uptake (Yeo et al., 1987; Ma and Peterson, 2003; Krishnamurthy et al., 2011; Kronzucker and Britto, 2011; Schreiber and Franke, 2011; Andersen et al., 2015; Barberon et al., 2016). While CSs are formed as radial wall thickenings, SLs are secondary wall thickenings on the inner face of primary cell walls (Schreiber et al., 1999; Naseer et al., 2012). Chemically, CSs are made up of mainly lignin and SLs are made up of suberin and/or lignin depositions (Schreiber et al., 1999;

[1]This work was supported by the Singapore National Research Foundation under its Environment and Water Research Programme (grant no. R–706–000–040–279).

[2]Present address: School of Biological Sciences, Nanyang Technological University, Singapore 637551.
[3]Author for contact: dbskumar@nus.edu.sg.
[4]Senior author.
The author responsible for distribution of materials integral to the findings presented in this article in accordance with the policy described in the Instructions for Authors (www.plantphysiol.org) is: Prakash P. Kumar (dbskumar@nus.edu.sg).

P.K. and P.P.K. conceived the research plans; P.K., H.W.J., F.C.J.L., and F.S.M.L. performed most of the experiments; B.V carried out rice experiments and gas chromatography-tandem mass spectrometry analysis; and P.K. designed the experiments, analyzed the data, and wrote the article with contributions from all the authors.

[OPEN]Articles can be viewed without a subscription.
www.plantphysiol.org/cgi/doi/10.1104/pp.20.01054

Naseer et al., 2012). Together, these barriers function in biotic and abiotic stress responses (Enstone et al., 2003; Krishnamurthy et al., 2009; Chen et al., 2011; Ranathunge et al., 2011a; Schreiber and Franke, 2011). Suberin is a biopolymer consisting of aliphatic and aromatic domains, with the aliphatic domain contributing mainly to its barrier properties (Kolattukudy, 1984; Schreiber et al., 1999; Ranathunge and Schreiber, 2011). Suberin biosynthesis is a complex pathway involving elongases, hydroxylases, and peroxidases (Bernards et al., 2004; Franke et al., 2005; Höfer et al., 2008; Franke et al., 2009). Cytochrome P450s (CYPs) are one of the largest superfamilies of peroxidases and are well characterized and known to carry out ω-hydroxylation of the aliphatic constituent of suberin, namely, ω-hydroxy acids (Höfer et al., 2008; Compagnon et al., 2009; Pinot and Beisson, 2011). Most of the CYPs that act on fatty acids belong to CYP86 and CYP94 subfamilies (Pinot and Beisson, 2011). Some of the CYPs, such as CYP86A1, CYP94A1, CYP94A2 and CYP94A5, have been identified as ω-hydroxylases (Franke and Schreiber, 2007; Höfer et al., 2008). Although the role of the CYP94B subfamily in initial ω-oxidation of jasmonoyl-Ile (JA-Ile) to 12-hydroxy-JA-Ile (12OH-JA-Ile), affecting JA signaling, is known (Koo et al., 2014; Bruckhoff et al., 2016), their role in suberin biosynthesis has not been explored so far and it would be desirable to examine the association between CYP94B members and root barrier formation.

There is limited information on the molecular mechanisms controlling the genes that regulate suberin biosynthesis. Overexpression of *MYB41* increases suberin biosynthesis as well as expression of some *CYP86* subfamily genes (Kosma et al., 2014). MYB39 regulates suberin deposition (Cohen et al., 2020). In addition, the promoter regions of *CYP83* and *CYP71* subfamilies have the W-box, a WRKY transcription factor (TF) binding domain (Xu et al., 2004; Birkenbihl et al., 2017). However, to the best of our knowledge, identities of TF(s) that regulate *CYP94B* subfamily genes are unknown.

In this study, we identified and functionally characterized a *CYP94B* subfamily gene, *AoCYP94B1*, from *A. officinalis* and its Arabidopsis (*Arabidopsis thaliana*) ortholog, *AtCYP94B1*. Expression of these genes was induced by salt treatment. We also show that heterologous expression of *AoCYP94B1* increased the salt tolerance and root suberin deposition in Arabidopsis and rice (*Oryza sativa*) seedlings. We visualized root suberin using histochemical staining and quantified suberin precursors in the *atcyp94b1* mutant using gas chromatography and tandem mass spectrometry (GC-MS/MS). Using mutant analysis, chromatin immunoprecipitation (ChIP), and yeast one-hybrid (Y1H) and luciferase assays, we demonstrated that AtWRKY33 regulates *AtCYP94B1*. Additionally, we demonstrated rescue of the reduced suberin and salt-sensitive phenotype by expressing *35S::AtCYP94B1* in *atwrky33*. Collectively, the data presented helped to identify the molecular regulatory mechanism involving apoplastic barrier formation through *CYP94B1*, which can be used as an important strategy for generating salt-tolerant crops.

RESULTS

Identification of *AoCYP94B1*, a *CYP94B* Subfamily Member from *A. officinalis*, as a Salt-Induced Gene

Several cytochrome P450 genes in the *CYP94B* subfamily, such as *AoCYP94B1* and *AoCYP94B3*, were identified in our earlier transcriptomic study of *A. officinalis* roots (Krishnamurthy et al., 2017). Since some reports (Benveniste et al., 2006) suggest a role for genes in this subfamily ω-hydroxylation, an important step in suberin biosynthesis, we chose *AoCYP94B1* for further characterization. A phylogenetic tree was constructed based on the derived amino acid sequence of *AoCYP94B1* with other members of this subfamily (Supplemental Fig. S1A). Rice OsCYP94B3 and Arabidopsis AtCYP94B1 were among the homologs that share a high level of sequence similarity with AoCYP94B1. AoCYP94B1 showed 60% identity and 74% similarity with AtCYP94B1, and 60% identity and 71% similarity with OsCYP94B3. The Cytochrome P450 Cys heme-iron ligand signature motif was conserved across various plant species (Supplemental Fig.S1B).

In *A. officinalis* seedlings without salt treatment, *AoCYP94B1* transcripts were constitutively expressed in all tissues, but higher levels of expression were observed in the leaves and stems compared to roots (Fig. 1A). The transcript levels in the roots increased 18-fold with 30 min of NaCl treatment and declined thereafter over 48 h (Fig. 1B). In the leaves, a 14-fold increase was seen after 4 h of NaCl treatment (Fig. 1B). In a parallel exploratory study, the Arabidopsis ortholog *AtCYP94B1* showed somewhat comparable expression patterns in all tissues tested except for flowers, where the increase was ~7-fold (Fig. 1C). The transcript level of *AtCYP94B1* was induced (~4-fold) by 30 min after salt treatment in the roots and remained high up to 6 h after treatment. In leaves, the expression peaked to ~4-fold after 6 h of salt treatment (Fig. 1D). Mimicking the reverse transcription quantitative PCR (RT-qPCR) expression profile, *pAtCYP94B1::GUS* expression was found in all tissues (Fig. 1, E and F) and increased by 30 min after salt treatment in the roots (Supplemental Fig. S2A). While *pAtCYP94B1::GUS* expression was mainly seen in the stele of the control roots, the expression significantly increased (~3-fold) in salt-treated roots and was mainly found in the endodermis (Fig. 1G and inset). Similarly, upon salt treatment, *pAtCYP94B1*-driven AtCYP94B1-GFP (Fig. 1, H and I) fusion localized to endodermal cells, where apoplastic barriers are formed.

Heterologous Expression of *AoCYP94B1* Increases Salt Tolerance in Arabidopsis and Rice Seedlings

To functionally characterize AoCYP94B1, we heterologously expressed the protein in the *atcyp94b1* Arabidopsis transfer DNA (T-DNA) insertional mutant background. There was a reduction in seedling root growth of all the genotypes tested after salt treatment

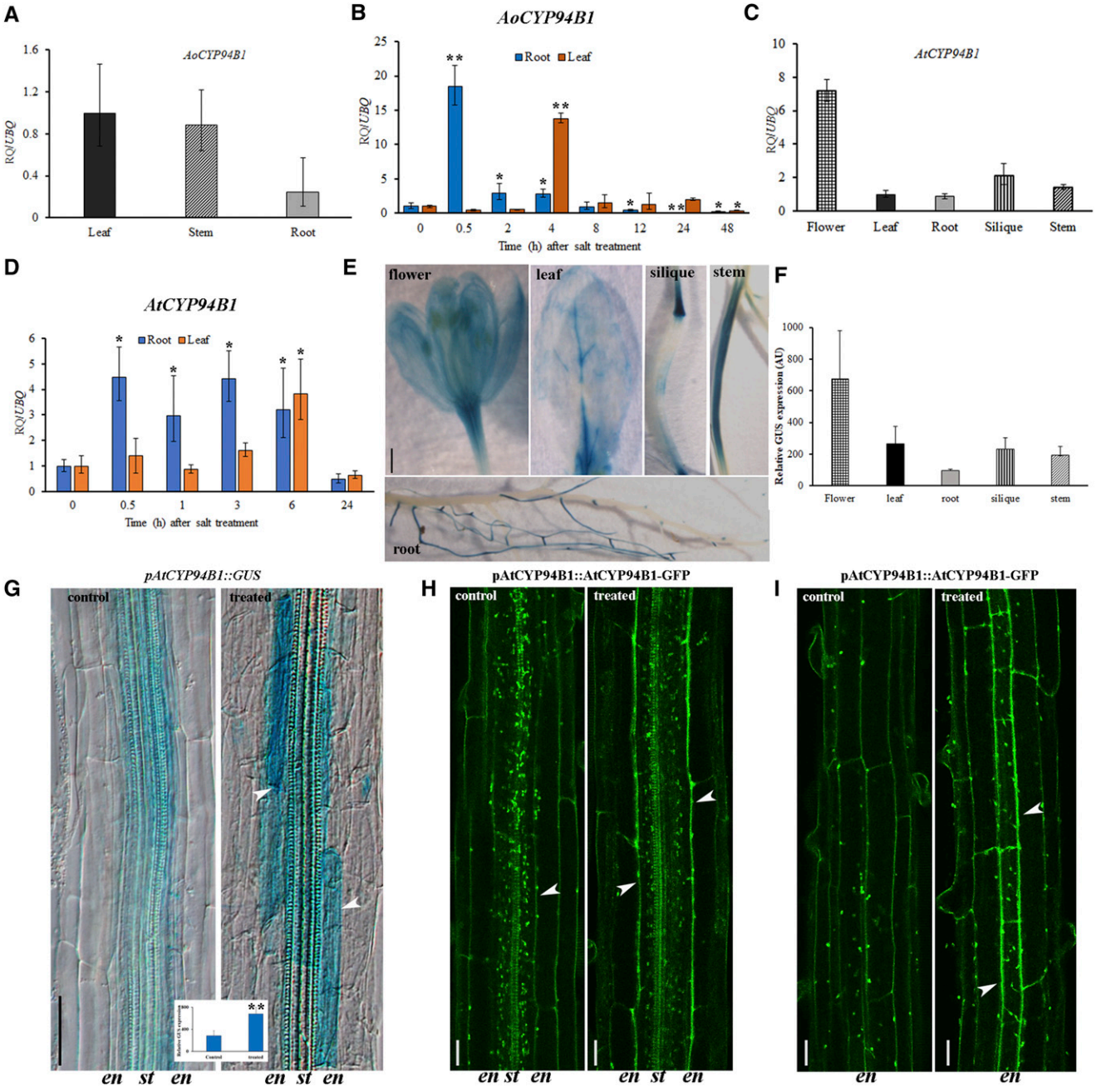

Figure 1. *CYP94B1* is induced by salt stress in both *A. officinalis* and Arabidopsis. A and B, Tissue-specific (A) and temporal (B) gene expression analyses by RT-qPCR of *AoCYP94B1* in roots and leaves of 2-month-old *A. officinalis* plants after 500 mM NaCl treatment for varying time periods. C, Tissue-specific expression of *AtCYP94B1* by RT-qPCR in 1-week-old Arabidopsis seedlings. D, Temporal expression of *AtCYP94B1* in roots and leaves after 50 mM NaCl treatment for varying time periods. Relative expression levels of transcripts with reference to *AtUBIQUITIN10* and *AoUBIQUITIN1* transcript levels are plotted in Arabidopsis and *A. officinalis*, respectively. RT-qPCR data represent means ± SD from three biological replicates each with three technical replicates. E, *pAtCYP94B1::GUS* expression in various tissues of mature plants bearing siliques. Scale bar = 500 μm. F, Relative quantification of *pAtCYP94B1::GUS* expression shown in E. G, Mature regions of roots showing *pAtCYP94B1::GUS* expression in control and salt-treated (50 mM NaCl for 3 h) 1-week-old Arabidopsis seedlings. Scale bar = 100 μm. Inset, Relative quantification of GUS intensity using ImageJ software plotted with the mean gray values normalized to the area. Data are the means ± SE of three biological replicates, each consisting of at least six plants. H and I, Median (H) and surface views (I) of *pAtCYP94B1*-driven AtCYP94B1-GFP (pAtCYP94B1::AtCYP94B1-GFP) expression in the root endodermal cells of control and salt-treated (50 mM NaCl for 24 h) 1-week-old Arabidopsis seedlings viewed under a confocal microscope. En, Endodermis; st, stele. Scale bar = 20 μm. Arrowheads in G to I show endodermal cells. Asterisks in graphs indicate statistically significant differences between control and treated seedlings (*$P < 0.05$ and **$P < 0.01$) as determined by Student's *t* test.

with 50 and 75 mM NaCl. However, *atcyp94b1* mutants showed about 53% and 76% reduction in root growth, respectively, compared to their untreated counterparts (Fig. 2). Under the same salt conditions, all three *35S::AoCYP94B1* lines tested grew better than the *atcyp94b1* mutant and the wild type (34% and 52% growth reduction with 50 and 75 mM salt treatment, respectively), showing 28%, 21%, and 17% reduction at 50 mM and 43%, 43%, and 40% reduction at 75 mM, respectively (Fig. 2). These data suggest that introduction of *35S::AoCYP94B1* into *atcyp94b1* increased its salt tolerance.

In addition, we examined salt sensitivity of 4-week-old plants grown in the soil to see if a similar salt response was evident in older plants. Under untreated conditions, there was no difference in the growth of the different genotypes. Upon NaCl treatment, *35S::AoCYP94B1* plants displayed better growth compared to the *atcyp94b1* plants (Fig. 3A; Supplemental Fig. S2B). Yellowing and drying of *atcyp94b1* leaves was evident, and they did not recover to the extent that wild-type and *35S::AoCYP94B1* lines did after the stress was withdrawn. While >80% of the wild-type and *35S::AoCYP94B1* lines showed survival (with more green and healthy leaves) after recovery growth, only 33% of *atcyp94b1* plants survived the treatment (Fig. 3B). There was no significant difference in leaf area among the genotypes, although a reduction in effective leaf area could be seen due to curling up of leaves upon salt treatment in all the genotypes (Fig. 3C). Other growth parameters, such as chlorophyll content and the fresh weight-to-dry weight (FW/DW) ratio, were generally reduced in all the genotypes upon salt treatment. While *atcyp94b1* mutants showed 3- and 4.5-fold reductions in chlorophyll content and the FW/DW ratio respectively, these reductions occurred to a lesser extent (~1.5-fold) in wild-type and *35S::AoCYP94B1* lines (Fig. 3, D and E). These observations suggest that introduction of *35S::AoCYP94B1* into *atcyp94b1* rescues its salt sensitive phenotype even in older plants.

We next measured the total Na^+ and K^+ ion contents in the leaves and roots of wild-type, mutant, and *35S::AoCYP94B1* plants under untreated and salt-treated (100 mM NaCl for 2 d) conditions to understand ion accumulation and distribution. There were no differences in the ion contents among the wild-type and transgenic lines in the absence of salt treatment (Fig. 3, F and G). Upon NaCl treatment, the amount of Na^+ increased from 1 to 38 mg g^{-1} DW in the leaves of *atcyp94b1* mutants, while in the *35S::AoCYP94B1* leaves, the amount was significantly lower (6, 8, and 7 mg g^{-1} DW in lines 1, 2, and 3, respectively; Fig. 3F). No significant differences were observed in the Na^+ and K^+ concentrations within the roots of the different genotypes tested (Fig. 3, F and G). These data indicate that the *35S::AoCYP94B1* lines efficiently controlled endogenous Na^+ accumulation in leaves.

Based on the observation that heterologous expression of *35S::AoCYP94B1* in Arabidopsis conferred increased salt tolerance, we expressed *pUBI::AoCYP94B1* in rice to examine whether a similar increase in salt tolerance could be conferred to the model crop species. There was no difference in the growth of wild-type and

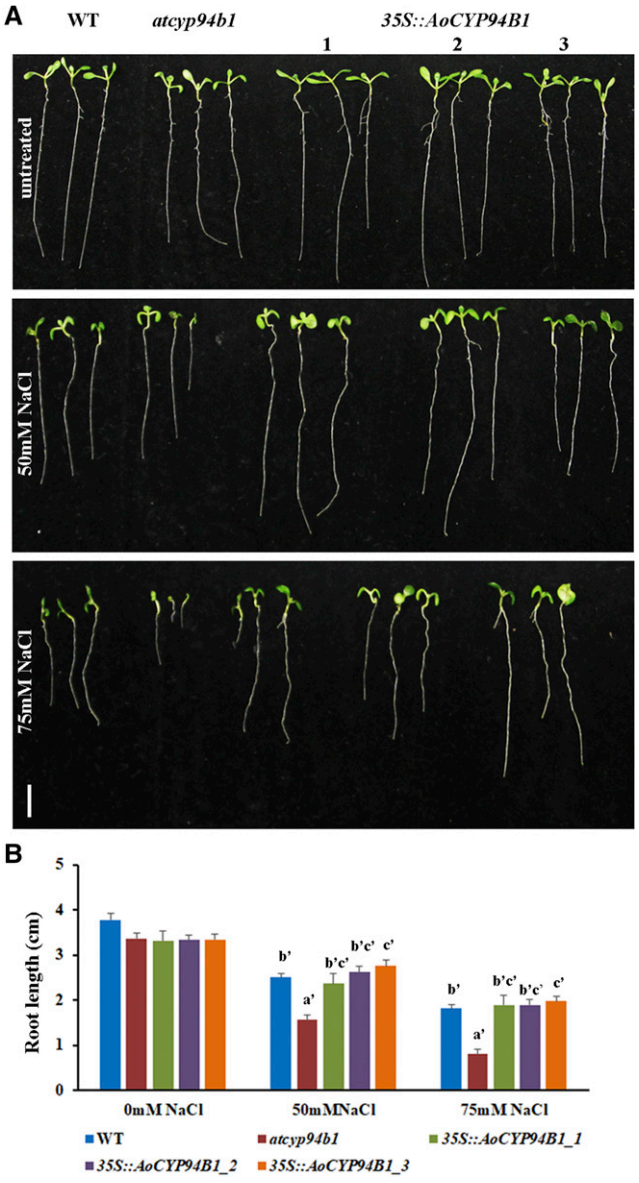

Figure 2. Heterologous expression of *AoCYP94B1* increases salt tolerance in Arabidopsis seedlings. A, Comparison of seedling growth among the wild type (WT), *atcyp94b1*, and three independent lines of *35S::AoCYP94B1* heterologously expressed in the mutant background. Scale bar = 10 mm. B, Root growth under salt treatment in wild-type, *atcyp94b1*, and *35S::AoCYP94B1* transgenic lines. Surface-sterilized and cold-stratified seeds were sown on Murashige and Skoog agar plates with or without NaCl (50 and 75 mM). Photographs and root length measurements were taken 1 week after germination. Data represent means ± SE of three independent experiments, each with at least 15 replicates per experiment. Different lowercase letters indicate statistically significant differences between genotypes as determined by ANOVA using Tukey-Kramer posthoc test ($P < 0.01$). Data sets without letters indicate no statistical difference.

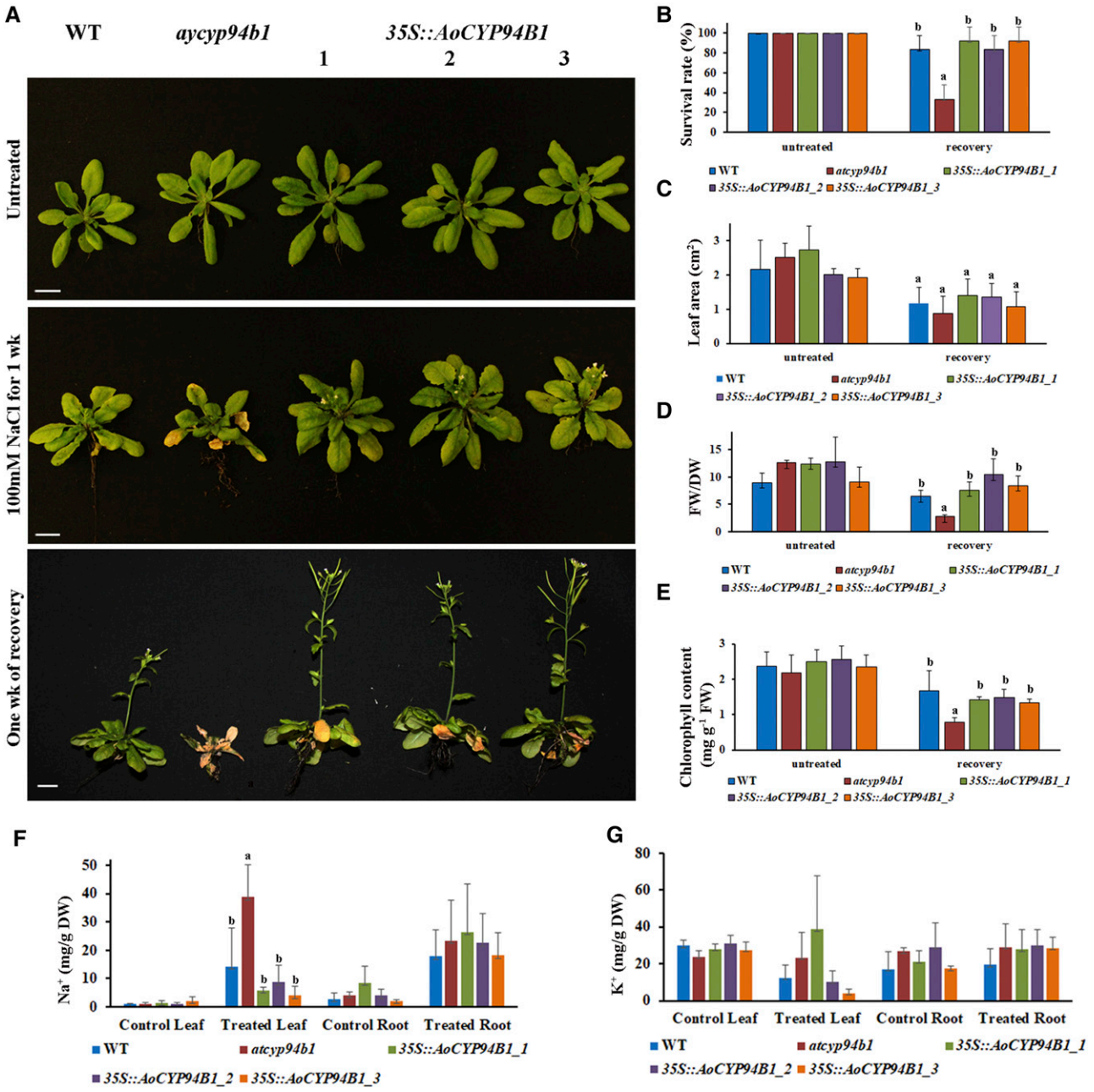

Figure 3. Heterologous expression of *AoCYP94B1* increases salt tolerance and regulates Na^+ accumulation in Arabidopsis plants. A, Growth response to salt (100 mM NaCl for 1 week) of the wild type (WT), *atcyp94b1*, and three independent lines of *35S::AoCYP94B1* heterologously expressed in the mutant background was monitored in 1-month-old, soil-grown Arabidopsis plants in the untreated and salt-treated conditions and after 1 week (wk) of recovery in normal water. Scale bar = 10 mm. B to E, Graphic representation of growth parameters such as survival rate ($n = 12$; B), leaf area ($n = 12$; C), FW/DW ratio ($n = 12$; D), and chlorophyll content ($n = 5$; E) for the plants shown in A. F and G, Total Na^+ content in the leaves and roots (F) and total K^+ content (G) in leaves and roots of 4-week-old wild-type, *atcyp94b1*, and three *35S::AoCYP94B1* lines. Data are means ± SE of three biological replicates, each consisting of at least three plants. Different lowercase letters indicate statistically significant differences between genotypes as determined by ANOVA using Tukey-Kramer posthoc test ($P < 0.05$). Data sets without letters indicate no statistical difference.

pUBI::AoCYP94B1 seedlings under untreated conditions (Fig. 4, A and B). However, the *pUBI::AoCYP94B1* rice seedlings showed significantly higher shoot and root growth compared to the wild-type after 3 and 6 d of 100 mM NaCl treatment on Murashige and Skoog agar plates (Fig. 4, C and D). Although growing the young seedlings is convenient on Murashige and Skoog medium, we sought to test the rice plants under hydroponic culture conditions normally used to simulate its natural growing environment. On salt treatment for 21 d, the hydroponically grown 1-month-old *pUBI::AoCYP94B1* seedlings showed about 35% higher survival rate compared to the wild type (Fig. 4, E and F). This further demonstrates that *AoCYP94B1* plays an important role in salt tolerance and could serve as an important candidate for improving salt tolerance of crops.

To gain further insight into the underlying molecular mode of action, we chose to work with the Arabidopsis ortholog. This allowed more detailed biochemical and molecular genetic analyses to be performed, which were not feasible with *A. officinalis*, a perennial tree species that is not amenable to genetic transformation.

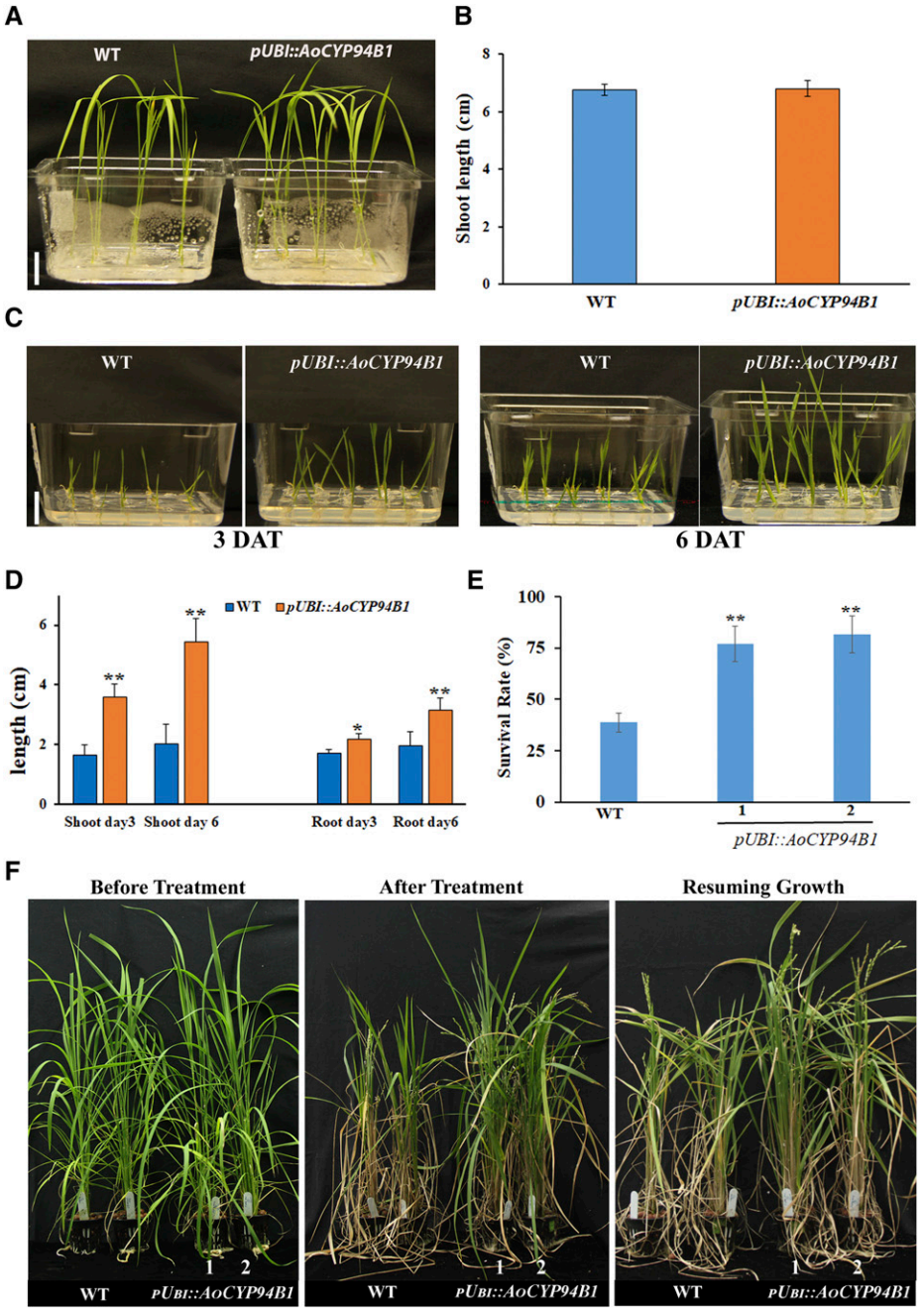

Figure 4. Heterologous expression of *AoCYP94B1* increases salt tolerance in transgenic rice seedlings. A, Phenotype of untreated 2-week-old wild-type (WT) and *pUBI::AoCYP94B1* seedlings. B, Shoot length of untreated wild-type and *pUBI::AoCYP94B1* seedlings. C, Phenotype of 1-week-old wild-type and *pUBI::AoCYP94B1* seedlings 3 and 6 days after treatment (DAT) with 100 mM NaCl. D, Shoot and root lengths of wild-type and *pUBI::AoCYP94B1* seedlings 3 and 6 DAT. E, Survival rates of wild-type and *pUBI::AoCYP94B1* plants after salt treatment and recovery growth. F, Four-week-old hydroponically grown wild-type and *pUBI::AoCYP94B1* plants before salt treatment, after 21 d of 100 mM NaCl treatment, and after an additional 10 d of recovery growth. Data in B, D, and E are means ± SD of three independent experiments, with at least 15 seedlings per experiment. Asterisks indicate statistically significant differences (**$P < 0.01$) between *pUBI::AoCYP94B1* and the wild type as measured by Student's *t* test. Scale bars = 1 cm.

AtCYP94B1 Increases Salt Tolerance as Well as SL Formation in Arabidopsis Roots

Similar to the *AoCYP94B1* heterologous expression lines, *pAtCYP94B1::AtCYP94B1* complementation lines showed better seedling root growth compared to the *atcyp94b1* mutants when subjected to 50 and 75 mM NaCl treatment (Fig. 5, A–D), indicating that the salt-sensitivity phenotype of *atcyp94b1* mutants was rescued in the *pAtCYP94B1::AtCYP94B1* complementation lines. Analysis was carried out in three *pAtCYP94B1::AtCYP94B1* complementation lines, and two representative lines are shown in Figure 5, A to C. However, mannitol treatment, an alternative abiotic stress, did not cause significant changes to the seedling root growth in any of these genotypes (Supplemental Fig. S3).

In view of the suggested role for *CYP94B* family genes in suberin biosynthesis, combined with our observation of reduced Na^+ accumulation in the shoots of *35S::AoCYP94B1* lines, we carried out GC-MS/MS quantification of several aliphatic components of the root suberin monomers in the wild type, *atcyp94b1*, *pAtCYP94B1::AtCYP94B1* complementation lines, and *35S::AoCYP94B1* heterologous expression lines. The *atcyp94b1* mutant showed a significant reduction in the amount of ω-hydroxy acids and α,ω-dicarboxylic acid compared to the other genotypes tested (Fig. 5E). No significant differences in the amounts of p-coumaric acid, C-18 octadecanoic acid, and C-22 docosanol were found between the genotypes tested. While *atcyp94b1* showed ~50% reduction in the amounts of alcohols (C-18 octadecanol and C-20 eicosanol), ω-hydroxy acids (C-16 and C-22), and C-16 α,ω-dicarboxylic acid (Fig. 5E), the levels of all except C-18 octadecanol were restored to wild-type levels in *pAtCYP94B1::AtCYP94B1* complementation lines. The increase of C-18 octadecanol,

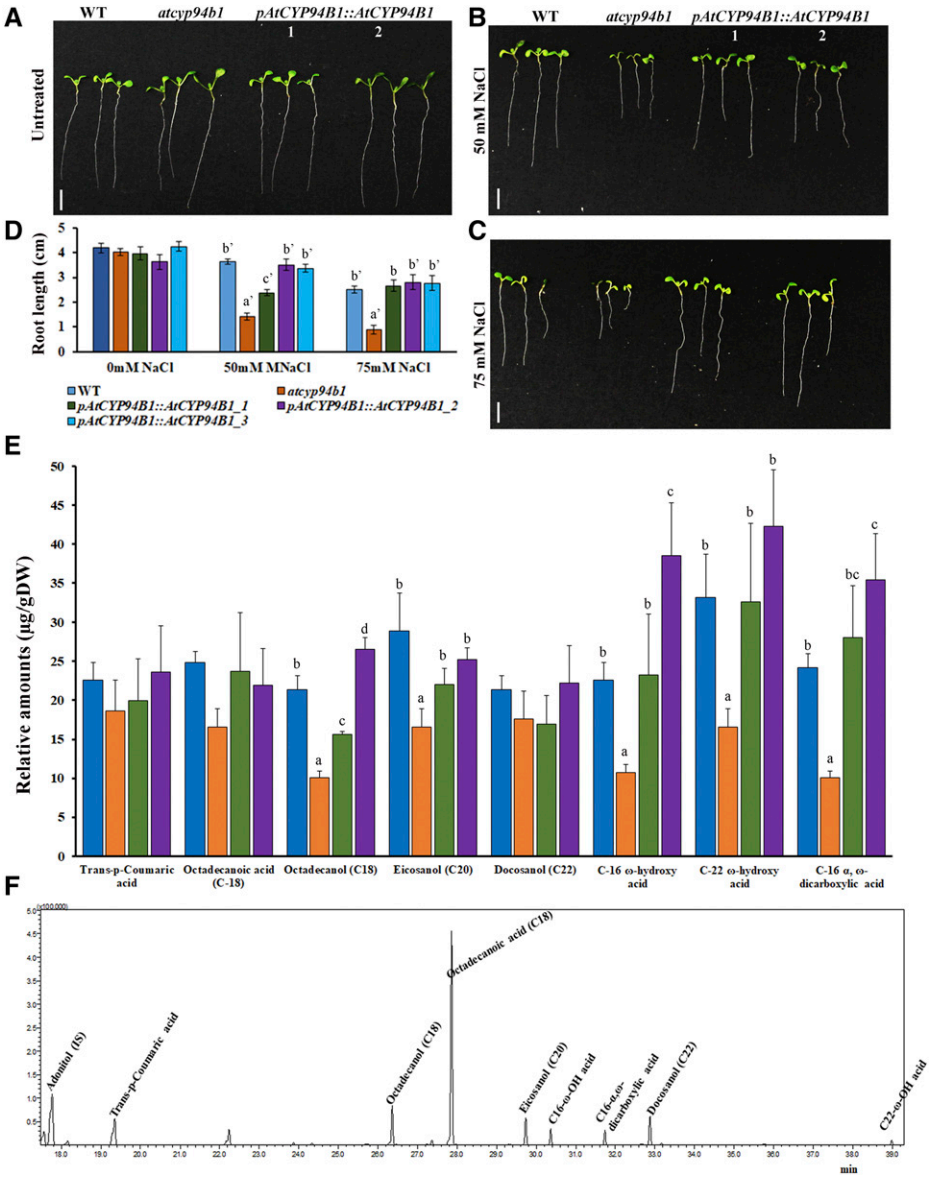

Figure 5. Complementation of *atcyp94b1* with Arabidopsis *AtCYP94B1* increases salt tolerance and suberin levels in Arabidopsis roots. A to C, Comparison of seedling growth among the wild type (WT), *atcyp94b1*, and two independent complementation lines of *pAtCYP94B1::AtCYP94B1* in the mutant background grown in 0 (A), 50 (B), and 75 mM (C) NaCl. Scale bars = 10 mm. D, Root growth under salt treatment in wild-type, *atcyp94b1*, and *pAtCYP94B1::AtCYP94B1* complementation lines. Surface-sterilized and cold-stratified seeds were sown on Murashige and Skoog agar plates with or without NaCl (50 and 75 mM). Photographs and root length measurements were taken 1 week after germination. Data are means ± SE of at least 15 biological replicates. Different letters indicate statistically significant differences between genotypes as determined by ANOVA using Tukey-Kramer posthoc test ($P < 0.01$). Data sets without letters indicate no statistical difference. E, Suberin monomer composition in the roots of 4-week-old wild-type, *atcyp94b1*, *pAtCYP94B1::AtCYP94B1*, and *35S::AoCYP94B1* seedlings was quantified by GC-MS/MS. Data are means ± SD of three independent biological replicates, each with four to five plants. Different lowercase letters indicate statistically significant differences between genotypes as determined by ANOVA using the Tukey-Kramer post-hoc test ($P < 0.05$). Data sets without letters indicate no statistical differences. F, Chromatogram (multiple reaction monitoring) of the standard suberin monomers and the internal standard (adonitol).

C-16 ω-hydroxy acids, and C-16 α,ω-dicarboxylic acid seen in *35S::AoCYP94B1* lines was higher than that of the wild type, which could be either due to the strength of the 35S promoter or because *AoCYP94B1* functions much more efficiently. The finding of significantly higher amounts of C-16 ω-hydroxy acid and C-16 α,ω-dicarboxylic acid in *35S::AoCYP94B1* lines compared to the wild type indicates a role for CYP94B1 in their biosynthesis. All the standards quantified for this study are shown in the chromatogram in Figure 5F.

Further, to visualize the altered suberin deposition in the roots, we carried out root histochemical studies in the wild type, *atcyp94b1*, *pAtCYP94B1::AtCYP94B1* complementation lines, and *35S::AoCYP94B1* heterologous expression lines. There was no difference in the deposition of root CSs among the genotypes (Fig. 6B). However, there was a significant reduction in the deposition of suberin in the endodermal cell walls of *atcyp94b1* compared to wild-type, *pAtCYP94B1::AtCYP94B1*, and *35S::AoCYP94B1* roots. While SLs were found in ~70% of the endodermal cells in the wild type, *pAtCYP94B1::AtCYP94B1*, and *35S::AoCYP94B1*, only 20% of cells in *atcyp94b1* exhibited SLs (Fig. 6, C–E). The patchy zones of *35S::AoCYP94B1_1* roots contained a significantly higher number of endodermal cells with suberin compared to wild type and *atcyp94b1* (Fig. 6, C and E). Furthermore, we examined the uptake of fluorescein diacetate (FDA), which is used as a tracer to check the barrier properties of SLs (Barberon et al., 2016). In the undifferentiated (CSs not formed) and nonsuberized (well-formed CSs) zones of the roots of all the genotypes checked, FDA entered all endodermal (100%) as well as pericycle cells after 1 min of incubation (Supplemental Fig. S4, A–D). However, in the suberized zones of the roots, FDA penetrated only ~10% of endodermal cells in the wild type, *pAtCYP94B1::AtCYP94B1*, and *35S::AoCYP94B1*, while it entered ~80% of *atcyp94b1* endodermal cells (Fig. 5, F and G). In addition, to check whether the enhanced salt tolerance in rice was caused by a similar mechanism, namely, increased SL deposition as seen in Arabidopsis, we examined the salt-treated roots of wild-type and *pUBI::AoCYP94B1* rice lines. In the apical regions, SLs were visible in a higher number of endodermal cells in *pUBI::AoCYP94B1* than in the wild type. In the mid-regions, SLs were clearly visible in *pUBI::AoCYP94B1*, while several endodermal cells lacked SLs in the wild type. In the basal regions, SLs were prominent in all the endodermal cells of *pUBI::AoCYP94B1*, while many passage cells without SLs were evident in the wild type (Supplemental Fig. S5, A and B). SL deposition showed a trend in the exodermal layer similar to that in the endodermis (Supplemental Fig. S5, C and D). These results not only suggest that *AtCYP94B1* has a critical role in the formation of SL as the apoplastic barrier leading to salt tolerance, but also that *AoCYP94B1* could function similarly to its Arabidopsis ortholog. Therefore, the use of *AtCYP94B1* for further understanding of its molecular regulatory mechanism can be justified.

Identification of the AtWRKY33 Transcription Factor as the Upstream Regulator of *AtCYP94B1*

We sought to identify the upstream regulator of *AtCYP94B1* in Arabidopsis after establishing the fact that *AoCYP94B1* and *AtCYP94B1* function in a similar manner to regulate root apoplastic barrier formation, leading to salt tolerance. Analysis of the 5′-upstream region of *AtCYP94B1* showed various abiotic stress-related cis-elements, such as WRKY, MYB, and MYC TF binding domains, and especially an enrichment of WRKY binding domains (Supplemental Fig. S6A). Coincidentally, in our earlier transcriptomic study, WRKYs (e.g. AoWRKY6, AoWRKY9, and AoWRKY33) were one of the major groups of TFs upregulated upon salt treatment in the roots of *A. officinalis* (Krishnamurthy et al., 2017). Because the role of WRKY33 in salt tolerance of plants has emerged in several studies, we selected AtWRKY33, which shares high sequence similarity to AoWRKY33 (Supplemental Fig. S7, A and B), for further study. Also, we used WRKY6 and WRKY9 belonging to Group I in ChIP and Y1H assays to ensure that the interaction and regulation were specific to WRKY33 (Group I WRKY).

We first conducted RT-qPCR analysis to check whether induction of *AtWRKY33* by salt treatment was similar to that of *AtCYP94B1*. Under untreated control conditions, we observed that *AtWRKY33* expression was comparable across tissue samples (Fig. 7A). In contrast, as seen for *AtCYP94B1* earlier, expression levels of *AtWRKY33* increased by 30 min after salt treatment in the roots and remained high (4-fold after 3 h) for up to 6 h (Fig. 7B). Similarly, in leaves, *AtWRKY33* expression increased 5-fold by 30 min after salt treatment (Fig. 7B). Furthermore, similar to the RT-qPCR expression profile, *pAtWRKY33::GUS* expression was seen in all tissues in untreated seedlings (Supplemental Fig. S8) and increased upon 50 mM NaCl treatment in the roots (Fig. 7, C and D). *pAtWRKY33::GUS* was mainly expressed in salt-treated Arabidopsis root endodermal cells (Fig. 7E), similar to *AtCYP94B1* expression.

To experimentally validate whether AtWRKY33 regulates *AtCYP94B1*, the expression level of *AtCYP94B1* was quantified in *atwrky33* mutants. *AtCYP94B1* transcript levels decreased 14-fold in *atwrky33* mutants (Fig. 7F). In addition, ChIP-qPCR analysis was performed to check for WRKY interaction with an *AtCYP94B1* promoter fragment. Consistent with the presence of putative WRKY-binding cis-elements, >10-fold enrichment of the *AtCYP94B1* promoter fragment was observed in AtWRKY33-HA pulldown samples (Fig. 7G). AtWRKY6-HA and AtWRKY9-HA pulldown was also carried out to check whether the interaction was specific to AtWRKY33, and there was no significant enrichment of AtCYP94B1 promoter fragments in these pulldown samples. We independently verified the interaction of AtWRKY33, AtWRKY6, and AtWRKY9 with the promoter fragment of *AtCYP94B1* using the Y1HGold system (Clontech). After introduction of

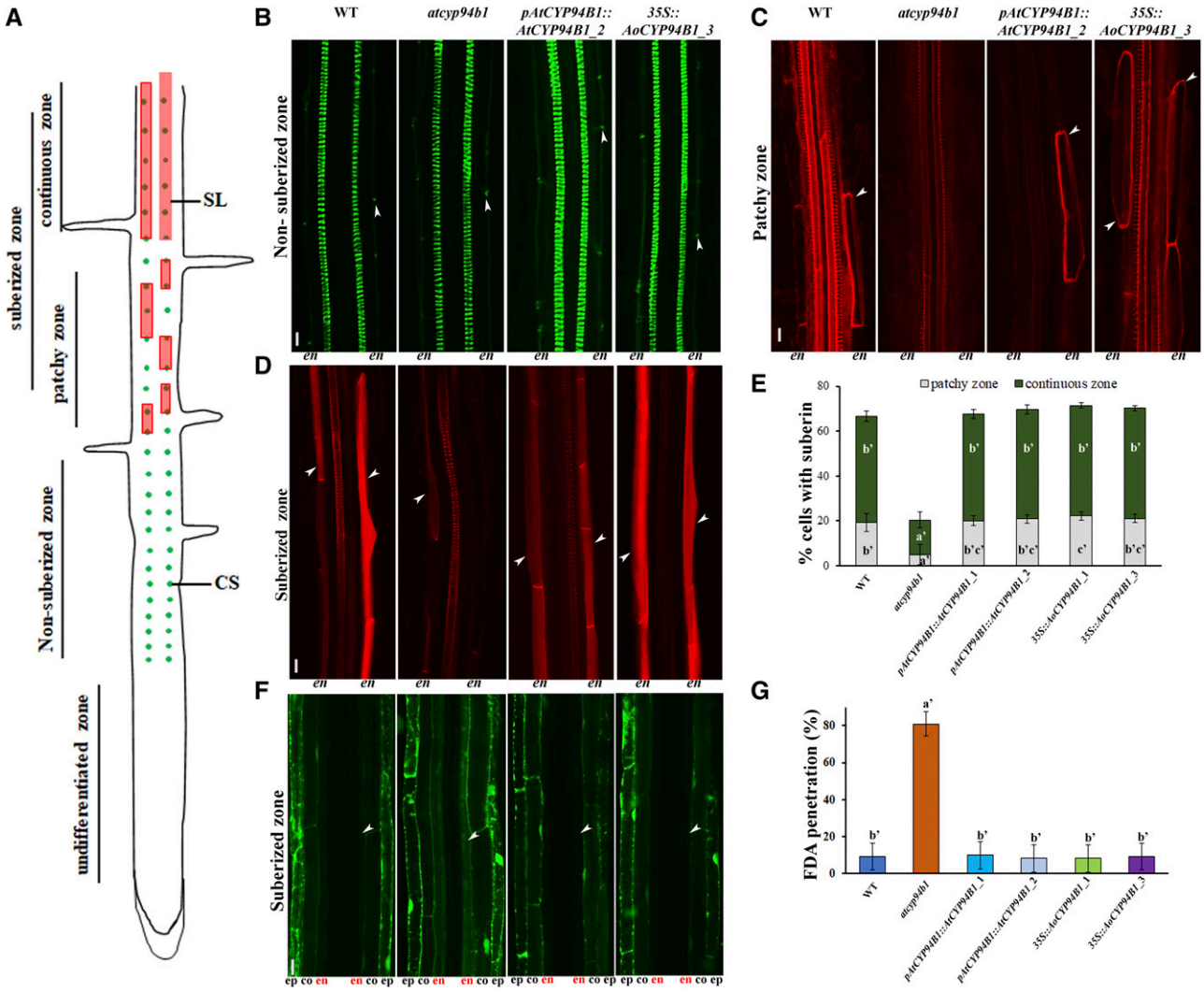

Figure 6. CYP94B1 is involved in apoplastic barrier (SL) formation in Arabidopsis roots. For root anatomical studies, 1-week-old Arabidopsis seedlings grown on Murashige and Skoog agar plates were used. Images were taken from similar parts of wild-type (WT), *atcyp94b1*, *pAtCYP94B1::AtCYP94B1*, and *35S::AoCYP94B1* stained roots. Seedlings were stained with Auramine O to visualize Casparian strips (CSs) and Nile Red to view suberin lamellae (SLs). Suberin patterns were counted as described in "Materials and Methods". A, Schematic of endodermal differentiation (adapted from Barberon et al., 2016). Three different zones are shown: suberized (with distinct patchy and continuous zones), nonsuberized, and undifferentiated. B, Representative images of CSs in the endodermis of nonsuberized zones of roots. C and D, Images showing SL deposition in the endodermal cells of patchy (C) and continuous (D) suberized zones of roots. Ep, Epidermis; co, cortex; en, endodermis (in red). Arrowheads indicate locations of CSs and SLs, except in F, where they show the endodermis. Scale bars = 10 μm. E, Percentage of endodermal cells with SLs in the suberized zones. n = 10 seedlings. F, FDA penetration after 1 min in the suberized root zones of wild-type, *atcyp94b1*, *pAtCYP94B1::AtCYP94B1*, and *35S::AoCYP94B1*. G, Percentage of endodermal cells with FDA penetration in the suberized zone. n = 10. Different lowercase letters indicate statistically significant differences between genotypes as determined by ANOVA using Tukey-Kramer posthoc test ($P < 0.01$). Same letters indicate no statistical difference.

pGADT7 AtWRKY33, *AtWRKY6*, and *AtWRKY9* plasmids into the Y1HGold cells harboring the *AtCYP94B1* promoter fragment, AtWRKY33 grew better than its control in the presence of Aureobasidin A (100 ng mL^{-1}), indicating an interaction between AtWRKY33 and the promoter of *AtCYP94B1* (Fig. 7H). While AtWRKY6 did not show any better growth compared to the control, there was very weak interaction with AtWRKY9 (Fig. 7H). Additionally, a luciferase assay using *atwrky33* Arabidopsis mutant protoplasts was carried out to check the in vivo transcriptional activation of the *AtCYP94B1* promoter by AtWRKY33. Protoplasts transfected with *pAtCYP94B1::LUC* along with *35S::AtWRKY33* showed ~3-fold higher luminescence compared to those transfected with the control, *pAtCYP94B1::LUC* (Fig. 7I). The mutant *pAtCYP94B1::LUC* (with two WRKY binding sites mutated) showed only ~1.5-fold higher luminescence compared to the control, indicating that

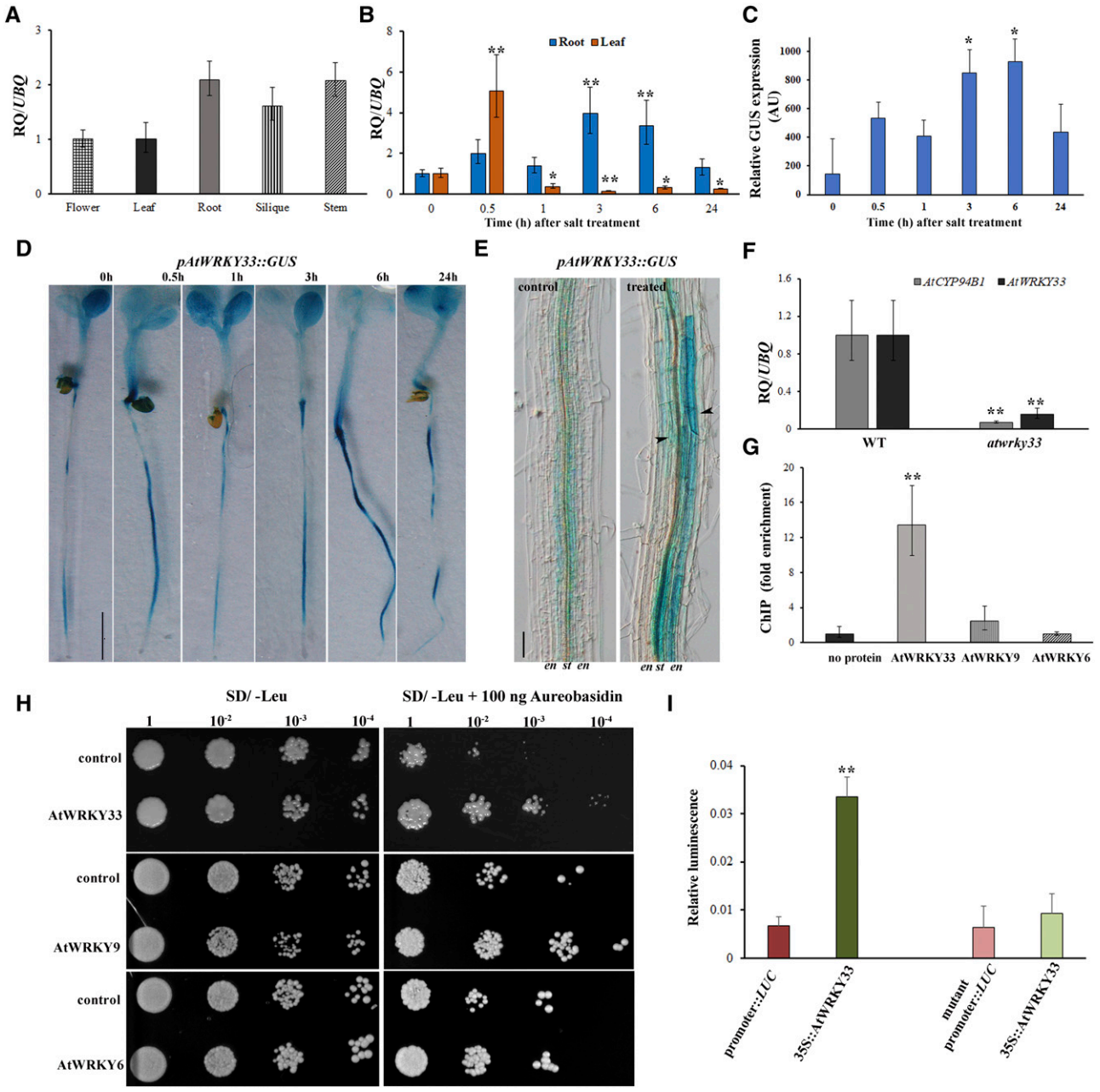

Figure 7. The AtWRKY33 transcription factor acts as an upstream regulator of *AtCYP94B1*. A and B, Tissue-specific (A) and temporal (B) gene expression analysis by RT-qPCR of *AtWRKY33* in roots and leaves of 1-week-old Arabidopsis seedlings after 50 mM NaCl treatment for varying time periods. RQ/UBQ, Relative quantification to *UBIQUITIN*. C and D, Relative GUS (C) and *pAtWRKY33::GUS* expression analysis (D) in 1-week-old seedling roots upon 50 mM NaCl treatment. Scale bar = 500 μm. Asterisks indicate statistically significant differences (*$P < 0.05$ and **$P < 0.01$) between 0 h and other time points as measured by Student's *t* test ($n = 6$). E, Root endodermal cells showing *pAtWRKY33::GUS* expression in control and salt-treated (50 mM NaCl for 6 h) 1-week-old Arabidopsis seedlings. Scale bar = 100 μm. Arrowheads show endodermal cells. en, Endodermis; st, stele. F, Transcript levels of *AtCYP94B1* in *atwrky33* T-DNA insertional mutant roots compared to wild-type (WT) roots. Asterisks indicate statistically significant differences (**$P < 0.01$) between the wild type and *atwrky33* as determined by Student's *t* test. Data represent means ± SD from three biological replicates, each with three technical replicates. G, ChIP-qPCR of HA-tagged AtWRKY33 in Arabidopsis protoplasts. AtWRKY6 and AtWRKY9 were used as negative controls. Fold change in the enrichment of promoter fragments compared to the no-protein control is plotted. Data represent means ± SD from three biological replicates, each with three technical replicates. Asterisks indicate statistically significant differences (**$P < 0.01$) between the no-protein control and AtWRKY33 as measured by Student's *t* test. H, Y1H assay showing regulation of *AtCYP94B1* by AtWRKY33. AtWRKY6 and AtWRKY9 were used as additional controls. The representative growth status of yeast cells is shown on SD/-Leu agar medium without and with 100 ng of aureobasidin A. Numbers above the photographs indicate relative densities of the cells

the mutation in the TF binding sites indeed affects the promoter activity. Collectively, these results show that AtWRKY33 TF acts as the upstream regulator of *AtCYP94B1*.

If the identified WRKY33 is indeed the upstream regulator of *AtCYP94B1* in vivo, root apoplastic barrier deposition in the *atwrky33* mutants should be impaired and expression of *35S::AtCYP94B1* in *atwrky33* mutant should rescue this phenotype. There were no visible differences in the formation of CSs in the *atwrky33* mutants compared to wild-type and *35S::AtCYP94B1 atwrky33* roots (Fig. 8A). However, suberin deposition was reduced in the roots of *atwrky33* compared to those of the wild type and *35S::AtCYP94B1 atwrky33* (Fig. 8B). While ~70% of wild-type and 60% of *35S::AtCYP94B1 atwrky33* endodermal cells showed SL deposition, only 25% of the corresponding *atwrky33* cells exhibited SL deposition (Fig. 8C). Further, the *atwrky33* mutant seedlings showed salt sensitivity similar to that shown by *atcyp94b1* mutants. However, this sensitivity was rescued when *35S::AtCYP94B1* was expressed in the *atwrky33* mutant background (Fig. 8D). These results strongly support our proposed working model where AtWRKY33 regulates root apoplastic barrier formation via *AtCYP94B1* to confer enhanced salt tolerance in plants (Fig. 8E).

DISCUSSION

It is imperative for researchers to understand the mechanisms underlying salt tolerance and generate salt-tolerant crops to meet the increasing demand for food to support the predicted population growth. Various studies have shown that apoplastic barrier deposition (mainly CSs and SLs) in the root endodermis and exodermis is critical to prevent unwanted loading of ions into the xylem (Krishnamurthy et al., 2011; Schreiber and Franke, 2011; Nawrath et al., 2013; Graça, 2015; Barberon, 2017; Kreszies et al., 2018). Although it is known that mangroves possess highly efficient apoplastic barrier deposition (Krishnamurthy et al., 2014), the underlying molecular mechanism is not well understood. The potential to learn from such adaptive mechanisms to devise strategies for crop improvement has been highlighted, but that is yet to be accomplished. This study represents a successful example of discovering and applying such mechanistic knowledge.

To understand the role of CYP94B1 in salt-stress response, we used three plant species (*A. officinalis*, Arabidopsis, and rice) of varying ages. Our earlier transcriptomic study involving *A. officinalis*, which led to the identification of *AoCYP94B1*, used 2-month-old seedlings treated with 500 mM NaCl (Krishnamurthy et al., 2017). Therefore, similar conditions were used for *A. officinalis* in this study. Experiments in Arabidopsis were carried out using young seedlings (1 week old) and older plants (4 weeks old) to understand their response to salt at two developmental stages. While 50 mM NaCl was used for most of the studies with younger seedlings, as this did not damage the roots, 100 mM NaCl was used to challenge the older plants. Similarly, two developmental stages in rice plants (1 and 4 weeks old) were used for our studies.

Our findings have highlighted the role of *AtCYP94B1* from Arabidopsis in the salinity tolerance response. This gene was identified as an ortholog of *AoCYP94B1* based on our studies with the mangrove tree, *A. officinalis*, which suggests that they may play similar roles in the two species. Under untreated conditions, expression of *AtCYP94B1* was lowest in roots, while it was predominant in flowers (Fig. 1C). A similar expression profile has been reported for *AtCYP94B1* in earlier studies (Bruckhoff et al., 2016; Widemann et al., 2016). However, according to the BAR eFP Browser, the highest expression occurs in petioles of mature leaves. Also, the *AtCYP94B1* gene family regulates flowering time but not fertility (Bruckhoff et al., 2016), while overexpression of *AtCYP94B3* leads to partial loss of male fertility in Arabidopsis (Koo et al., 2011). However, in our study, the ~4-fold upregulation of *AtCYP94B1* seen in the roots upon salt treatment (Fig. 1D), along with its expression and localization to the endodermis (Fig. 1, G–I) clearly indicates its key function in root endodermis under salt stress. While *AoCYP94B1* showed the highest expression at 0.5 h after salt treatment, *AtCYP94B1* expression remained high from 0.5 to 6 h. At this point, we are not sure whether this difference is a reflection of inherent differences between the two species or other factors.

Earlier studies suggest that CYP94B family genes, including AtCYP94B1, play a role in sequential ω-oxidation of JA-Ile to 12OH-JA-Ile (Koo et al., 2014; Aubert et al., 2015; Lunde et al., 2019), particularly after flower opening (Bruckhoff et al., 2016; Widemann et al., 2016). Those authors also highlight that a role for members of this CYP94 subfamily in metabolism of other substrates cannot be dismissed. Furthermore, in an earlier study, Arabidopsis CYP94B1 expressed in yeast carried out ω-hydroxylation of fatty acids with chain lengths of C12 to C18 (Benveniste et al., 2006). Accordingly, our observation that the reduction in the

Figure 7. (*Continued.*)
4 d postinoculation. I, Luciferase assay carried out using the mesophyll protoplasts obtained from leaves of 4-week-old *atwrky33* mutants. *pAtCYP94B1::LUC* was used as the control and *35S::AtWRKY33* was used as the test. The *AtCYP94B1* promoter fragment with mutated WRKY binding sites was used as an additional control. Firefly luciferase activity was normalized to *Renilla* luciferase activity and plotted. Data represent means ± SD of four independent biological replicates, each with three technical replicates. Asterisks indicate statistically significant differences between the control and the test (**$P < 0.01$) as measured by Student's *t* test.

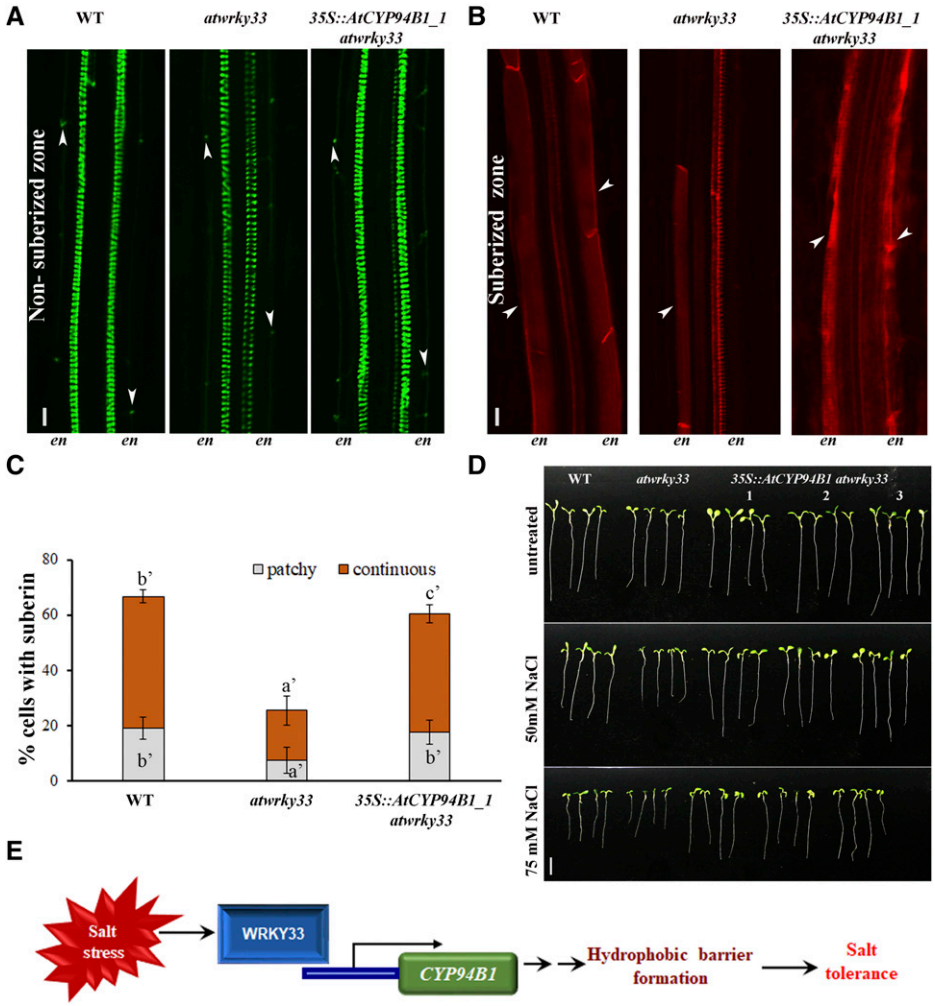

Figure 8. AtWRKY33 regulates apoplastic barrier formation via *AtCYP94B1*. For root anatomical studies, 1-week-old wild-type (WT), *atwrky33*, and *35S::AtCYP94B1 atwrky33* (in the *atwrky33* mutant background) Arabidopsis seedlings grown on Murashige and Skoog agar plates were used. Images of stained roots were taken from the same regions for all genotypes. Seedlings were stained with Auramin O for visualizing Casparian strips (CSs) and with Nile Red to view suberin lamellae (SLs). Suberin patterns were counted as described in "Materials and Methods". A, Representative images showing CS development in the nonsuberized endodermal cells of the three genotypes. B, SL deposition in the suberized endodermal cells of all three genotypes. C, Percentage of endodermal cells with SLs in the suberized zones of the roots. Arrowheads indicate locations of CSs and SLs. Scale bars = 10 μm, $n = 10$ seedlings. Different lowercase letters indicate statistically significant differences between genotypes as determined by ANOVA using Tukey-Kramer posthoc test ($P < 0.01$). Same letters indicate no statistical differences. en, Endodermis. D, Comparison of seedling growth among the wild type, *atwrky33*, and three independent lines of *35S::AtCYP94B1 atwrky33* ectopic expression lines. Surface-sterilized and cold-stratified seeds were sown on Murashige and Skoog agar plates with or without NaCl (50 and 75 mM). Photographs were taken 1 week after germination. Scale bar = 10 mm. E, Proposed model based on our data showing regulation of root apoplastic barrier formation by WRKY33 through control of *CYP94B1*, leading to salt tolerance.

concentration of aliphatic suberin monomers (C16 and C22 ω-hydroxyacids) in the roots of *atcyp94b1* mutants compared to the wild type, complementation, and heterologous expression lines (Fig. 5E) confirms the role of CYP94B1 in biosynthesis of aliphatic suberin monomers, leading to the formation of apoplastic barriers in the roots. The induction of *CYP94B1* gene expression by salt treatment in Arabidopsis and *A. officinalis* (Fig. 1), coupled with the observation of reduced apoplastic barrier formation in the root endodermis (Fig. 6), as well as salt sensitivity in the *atcyp94b1* mutant (Figs. 2–4), collectively show that *AtCYP94B1* plays a role in the salinity response. The fact that the salt-sensitive phenotype and the reduced levels of suberin in the endodermis of *atcyp94b1* are rescued in the transgenic Arabidopsis lines (*35S::AoCYP94B1* and *pAtCYP94-B1::AtCYP94B1*) further confirms the role of CYP94B1 in salt tolerance via suberin deposition. It is also clear from our data that the SLs in the endodermal cell walls function to block the apoplastic flow (Fig. 6F) and thereby limit the uptake of excess Na^+ into the shoots (Fig. 3F). Several prior studies have shown similar

increases in the concentration of aliphatic suberin monomers in response to salt stress, which limits the root apoplastic bypass flow (Ranathunge et al., 2005, 2008, 2011a; Krishnamurthy et al., 2009, 2011, 2014). The increased salt tolerance exhibited by the heterologous expression lines (*35S::AoCYP94B1*) of rice (Fig. 4) and Arabidopsis (Figs. 2 and 3) was directly associated with increased apoplastic barrier formation in the roots (Figs. 5 and 6; Supplemental Fig. S5), suggesting that the mangrove *AoCYP94B1* could be used to confer enhanced salt tolerance to crop plants. JA-Ile degradation/oxidation occurs under salt stress (Hazman et al., 2019), and this leads to increased salinity tolerance in rice (Kurotani et al., 2015). Therefore, the role of this pathway in contributing to salt tolerance in our overexpression lines cannot be dismissed and demands further study to understand the relationship between JA catabolism and suberin biosynthesis under salt stress.

Suberin deposition occurs not only in response to abiotic stresses such as salinity and drought (Ranathunge et al., 2011b; Franke et al., 2012), but also to biotic stresses, where it serves to block pathogen entry through the cell walls (Ranathunge et al., 2008). Despite its pivotal role in conferring tolerance to multiple stresses, information on molecular regulation of apoplastic barrier formation is still scarce. So far, some of the MYB TFs have been shown to regulate CS development (Kosma et al., 2014; Kamiya et al., 2015; Li et al., 2018) and suberin biosynthesis (Gou et al., 2017) by regulating *CYP86* subfamily genes. To the best of our knowledge, no prior report on regulation of *CYP94B* subfamily genes exists. Salt-mediated coinduction of *AtWRKY33* (Fig. 7, B–D) with *AtCYP94B1* (Fig. 1D) and the endodermal expression of both *pAtCYP94B1::GUS* and *pATWRKY33::GUS* in the salt-treated roots (Figs. 1 and 7) suggest that they play a related role under salt treatment. This, combined with enrichment of *AtCYP94B1* promoter fragments in our ChIP-qPCR, Y1H analysis, and luciferase assay (Fig. 7) clearly show that AtWRKY33 is the upstream regulator of *AtCYP94B1*. WRKY TFs are known to regulate biotic (Bakshi and Oelmüller, 2014; Sarris et al., 2015) and abiotic stress responses (He et al., 2016; Liang et al., 2017; Bai et al., 2018), and several transcriptomic and microarray studies have shown their response to salt and drought stresses (Mahalingam et al., 2003; Narusaka et al., 2004; Krishnamurthy et al., 2011; Okay et al., 2014; Song et al., 2016). Additionally, overexpression of WRKY25, WRKY33, WRKY41, and WRKY83 causes enhanced salt tolerance (Jiang and Deyholos, 2009; Chu et al., 2015; Wu et al., 2017), while many others (WRKY46, WRKY54, WRKY68, and WRKY70) play a role in drought tolerance (Chen et al., 2017). However, the mechanism by which these WRKY TFs confer stress tolerance is not known. Our observations of reduced deposition of SLs in the endodermal cells of *atwrky33* mutants, mimicking the *atcyp94b1* mutant phenotype, along with the increase in SL deposition in the *35S::AtCYP94B1 atwrky33* lines (Fig. 8), further confirm the regulatory role of the AtWRKY33 TF on *AtCYP94B1*. Hence, we propose a working model where WRKY33 regulates root apoplastic barrier formation by controlling *CYP94B1*, leading to increased salt tolerance (Fig. 8E).

In conclusion, our study reveals part of an important molecular regulatory mechanism of suberin deposition that involves the control of *AtCYP94B1* by the AtWRKY33 TF, leading to increased salt tolerance of Arabidopsis seedlings. We further showed that heterologous expression of *AoCYP94B1* in both Arabidopsis and rice seedlings confers salt tolerance by the same mode of action. Therefore, our study opens new avenues for engineering salt-tolerant crop plants.

MATERIALS AND METHODS

Cloning and Generation of Transgenic Lines

The full-length coding sequence (CDS) of *AoCYP94B1* (Unigene99608_All) was obtained from an earlier transcriptomic study of *Avicennia officinalis* roots (Krishnamurthy et al., 2017). Wild-type Arabidopsis (*Arabidopsis thaliana*), ecotype Columbia-0, along with the T-DNA insertional mutants *atcyp94b1* (SALK_129672) and *atwrky33* (SALK_064436), were purchased from the Arabidopsis Biological Resource Center (http://www.abrc.osu.edu; Alonso et al., 2003). Position of T-DNA insertion sites for *atcyp94b1* and a*twrky33* mutants are shown in Supplemental Figs. S9 and S10, respectively. Genomic DNA from the mutants was extracted as described previously (Dellaporta et al., 1983). Plants homozygous for the T-DNA insertion were selected by genotyping with primers designed using the T-DNA primer design tool (http://signal.salk.edu/tdnaprimers.2.html). Also, RT-qPCR was carried out to check the suppression of the tagged gene expression in mutants (Supplemental Figs. S9 and S10). Seeds were collected only from those mutants that showed >70% reduction in *AtCYP94B1* as well as *AtWRKY33* expression (Supplemental Figs. S9C and S10C). For heterologous expression of *AoCYP94B1* in Arabidopsis, the CDS of *AoCYP94B1* was amplified and cloned into the pGreen binary vector under the 35S promoter using *Eco*RV and *Spe*I restriction sites. For construction of translational fusion with GFP and complementation lines of *AtCYP94B1*, the full-length cassette, including promoter, introns, and exons of *AtCYP94B1* amplified from the genomic DNA of Arabidopsis, was cloned into pGreen-GFP and pGreen binary vectors, respectively, using *Kpn*I and *Xma*I restriction enzyme sites. For promoter GUS expression analysis, 1-kb upstream sequences of *AtCYP94B1* and *AtWRKY33* were amplified from genomic DNA and cloned into pGreen-GUS using *Pst*I, *Xma*I and *Hin*dIII, *Xma*I restriction enzyme sites, respectively. All the constructs generated were individually electroporated into *Agrobacterium tumefaciens* strain GV3101:pMP90 and introduced into Arabidopsis by the floral dip method (Clough and Bent, 1998). Basta-resistant T1 transgenic plants were selected and introduced gene expression was confirmed by genotyping PCR and RT-qPCR analysis (Supplemental Fig. S9D). T3 generation plants were used for all the experiments. For ChIP, CDSs of *AtWRKY33*, *AtWRKY9*, and *AtWRKY6* were cloned into pGreen binary vector with the hemagglutinin (HA) fusion tag with the following restriction enzyme sites; *Eco*RI, *Spe*I for *AtWRKY33* and *AtWRKY9*, and *Xma*I, *Spe*I for *AtWRKY6*. For heterologous expression in rice (*Oryza sativa*), the CDS of *AoCYP94B1* was amplified and cloned with AvrII and *Xma*I restriction enzyme sites into binary vector pCAMBIA-1300 under the maize (*Zea mays*) *UBIQUITIN* promoter. The constructs were introduced into rice by *A. tumefaciens*-mediated transformation (Toki et al., 2006). Homozygous transgenic lines (3:1 segregation ratio on hygromycin selection) at the T2 generation were selected for further analysis. All primers used in this study are listed in Supplemental Table S1.

Plant Materials and Growth Conditions

The propagules of *A. officinalis* were collected during fruiting seasons from the mangrove swamps in Singapore (Berlayer Creek and Sungei Buloh Wetland Reserve). The seedlings were maintained in NaCl-free conditions by growing in potting mixture (Far East Flora) until they reached the four-node stage (~2 months) in a greenhouse (25°C to 35°C, 60% to 90% relative humidity; 12-h

photoperiod), after which they were carefully transferred to pots containing sand and were allowed to adapt for 2 d by watering with one-half strength Hoagland's solution. The plants were then treated with one-half strength Hoagland's solution containing 500 mM NaCl for varying time periods (0, 0.5, 1, 2, 4, 8, 12, 24, and 48 h).

For growth on Murashige and Skoog agar plates, Arabidopsis seeds of the required genotypes were surface sterilized and cold stratified at 4°C for 3 d, then sown on Murashige and Skoog agar plates and germinated at 22°C under continuous light. One-week-old seedlings were carefully removed from the plate and subjected to salt (50 mM NaCl) treatment. The plant tissues were collected at various time periods (0, 0.5, 1, 3, 6, and 24 h) and frozen in liquid nitrogen for total RNA isolation. For histochemical GUS expression analysis, 1-week-old seedlings were treated with 50 mM NaCl for various time periods (0, 1, 3, 6, and 24 h). For root length studies, the sterilized and cold-stratified seeds were sown on Murashige and Skoog agar plates with and without NaCl and root length was measured and photographed 1 week after germination. For salt treatment in older plants, 4-week-old plants were treated with 100 mM NaCl for 1 week. The pots were flushed with water twice to remove the soil-bound NaCl followed by a recovery growth in NaCl-free water for 1 week. Survival rate, chlorophyll contents, FW/DW ratio, and leaf area were measured from untreated and recovered plants. In addition, untreated plants bearing mature siliques were collected for RT-qPCR analysis and GUS staining.

Rice seeds of wild-type (ssp. *japonica* 'Nipponbare') and heterologous expression lines (*pUbi::AoCYP94B1*) were first germinated on plain Murashige and Skoog or selection medium (MS + hygromycin) and then transferred to Murashige and Skoog agar plates with and without NaCl (100 mM NaCl). After 1 week of growth in this medium, seedlings were photographed and the shoot and root lengths were measured. The wild-type and transgenic lines generated were grown hydroponically (Yoshida et al., 1971) for salt treatment of older seedlings. Four-week-old seedlings were subjected to salt treatment (100 mM NaCl) for 21 d. After treatment, the rice seedlings were transferred back to NaCl-free hydroponic solution for recovery. Survival rates were calculated after 10 d of recovery and are shown (Fig. 4E) as the percentage of seedlings that were alive. Plants that did not show any indication of recovery (no green shoots) were counted as dead.

In Silico Analysis

The NCBI database was used as a search engine for nucleotide and protein sequences. The expasy tool (https://web.expasy.org/translate/) was used to translate the CDS sequences to amino acid sequences, and multAlin (http://multalin.toulouse.inra.fr/multalin/) was used to align the amino acid sequences. Phylogenetic analysis was carried out using Phylogeny.fr software (http://www.phylogeny.fr/). Primers for RT-qPCR were designed using NCBI (https://www.ncbi.nlm.nih.gov/tools/primer-blast/).

RNA Isolation and RT-qPCR Analysis

RNA was isolated from various plant samples (*A. officinalis*, Arabidopsis, and rice) using TRIzol reagent (Thermo Fisher) according to the manufacturer's instructions. An aliquot of this RNA (1 μg) was used to synthesize complementary DNA (cDNA) using a Maxima first-strand cDNA synthesis kit for RT-qPCR (Thermo Fisher) and following the manufacturer's instructions. For genotyping of mutants and the heterologous expression lines, RNA was extracted from leaves of 4-week-old seedlings. RT-qPCR was performed to check expression of transcript levels using a StepOne Real-Time PCR machine (Applied Biosystems) with the following program: 20 s at 95°C followed by 40 cycles of 3 s at 95°C and 30 s at 60°C. The SYBR Fast ABI Prism PCR kit (Kapa Biosystems) was used for RT-qPCR analysis. The reaction mixture consisted of 5.2 μL master mix (provided in the kit), 0.2 μM each of forward and reverse primers, 3.4 μL nuclease-free water, and 1 μL sample cDNA template for a final volume of 10 μL. All data were analyzed using StepOne Software (version 2.1, Applied Biosystems). The primers used for RT-qPCR analysis are listed in Supplemental Table S1. Gene expression levels were calculated based on $\Delta\Delta$Ct values and presented as expression levels (fold change) relative to the constitutively expressed internal controls *AtUBIQUITIN10* and *AoUBIQUITIN1* for Arabidopsis and *A. officinalis*, respectively.

Chlorophyll Estimation

Chlorophyll concentrations were determined spectrophotometrically using 100 mg FW of untreated and recovered (from NaCl treatment) leaf material ground in 2 mL of 80% (v/v) acetone. After complete extraction, the mixture was filtered and the volume adjusted to 5 mL with cold acetone. The absorbance of the extract was read at 663 and 645 nm and pigment concentrations were calculated as described previously (Arnon, 1949). The data represented are means ± SD of four biological replicates each with single plants.

Estimation of Total Ion Concentration (Na^+ and K^+) from Plants

Control and salt-treated 4-week-old Arabidopsis seedlings were harvested and rinsed briefly with distilled water to remove surface-contaminating Na^+. Three to four plants were pooled as one replicate, and three to four independent replicates were used to generate the mean values reported. Leaves and roots from plants were separated and left to dry at 50°C for 2 d. The dried tissue was ground into a powder in liquid nitrogen, and acid digestion and ion estimation were carried out as described earlier (Krishnamurthy et al., 2014). The amounts of ions estimated are presented as milligrams per gram DW of plant sample.

Histochemical GUS Staining

Transgenic Arabidopsis seedlings containing *pAtCYP94B1::GUS* and *pAtWRKY33::GUS* fusion constructs were treated as described above. GUS histochemical staining was performed by vacuum infiltrating the seedlings immersed in GUS staining solution (0.1 M sodium phosphate buffer [pH 7.0], 10 mM EDTA, 0.1% [w/v] Triton X-100, and 2 mM 5-bromo-4-chloro-3-indolyl glucuronide) for 5 min followed by overnight incubation in the dark at 37°C without shaking. Staining solution was removed, and several washes with 50% (v/v) ethanol were performed until the chlorophyll was bleached and tissues cleared. The images of stained whole seedlings with various salt treatments were recorded using a stereo microscope (SMZ1500, Nikon), and other *pAtCYP94B1::GUS* images were taken using a CTR5000 DIC microscope (Leica) with a Nikon DS-Ril camera. GUS-stained images presented here represent the typical results of at least six independent plants for each treatment. GUS expression was quantified based on the relative intensities of blue coloration using ImageJ software (https://imagej.nih.gov/ij/download.html). Data presented are the means ± SD of three biological replicates, each biological replicate consisting of at least six plants.

Chemical Analysis of Suberin in the Root

Isolation and depolymerization of suberized root cell walls from 4-week-old Arabidopsis seedlings were carried out as described previously (Franke et al., 2005; Höfer et al., 2008). Briefly, the samples were depolymerized by transesterification with 2 mL 1 M MeOH/HCl for 2 h at 80°C followed by addition of salt water. Ten micrograms of adonitol was added as an internal standard, and aliphatic monomers were extracted three times in 0.5 mL of hexane. The combined organic phase was dried using CentriVap Cold Traps (Labconco) and derivatized using bis-(N,N,-trimethylsilyl)-trifluoroacetamide (Sigma-Aldrich) as described previously (Franke et al., 2005; Höfer et al., 2008). Monomers were identified from their electron ionization-MS spectra (75 eV, *m/z* 50–700) after capillary GC (30 m × 0.32 mm, 0.1 μm, on column injection at 50°C, oven 2 min at 50°C, 10°C min^{-1} to 150°C, 1 min at 150°C, 5°C min^{-1} to 310°C, 30 min at 310°C using 2 mL min^{-1} He carrier gas) on a gas chromatograph (DB-5MS, Shimadzu) combined with a quadrupole mass selective detector (GCMS-TQ80). Quantitative analysis of suberin monomers was carried out based on normalization to the internal standard. Three biological replicates, each consisting of four to five plants from all the genotypes tested, were used for the analysis. Suberin amounts are presented as micrograms per gram DW of the sample.

Histochemical Staining and Microscopy

For root histochemical studies, 1-week-old Arabidopsis seedlings grown on Murashige and Skoog agar were used. Seedlings were stained with Auramine O and Nile Red to visualize CSs and SLs, respectively, using the methods described earlier (Ursache et al., 2018). For CS development, cells from the first CS appearance to the first elongated cell were checked. As described previously (Barberon et al., 2016), suberin patterns were counted from the hypocotyl junction to the onset of endodermal cell elongation (i.e. the zone where an endodermal cell length is clearly more than twice its width). The roots were divided into various zones (Fig. 6A), such as the undifferentiated zone (young part of the root with no CS or SL), nonsuberized zone (only CSs, no SLs), and

suberized zone (patchy and continuous SLs). For FDA transport assay, seedlings were incubated for 1 min in one-half strength Murashige and Skoog FDA (5 μg mL^{-1}), rinsed, and observed using a confocal laser scanning microscope (FV3000, Olympus). Excitation and detection parameters were set as follows: Auramine O, 488 nm and 505 to 530 nm; Nile Red, 561nm and 600 to 650 nm; FDA, 488 nm and 620 to 640 nm. Images were taken from at least 10 Arabidopsis seedlings of each genotype tested for all the analyses.

For microscopy of rice roots, freehand cross sections were prepared from the adventitious roots of salt-treated rice plants grown in hydroponics. Roots~100 mm in length were taken from the hydroponically grown, salt-treated plants and sectioned at varying lengths from the root tip: apical (0–20 mm), mid- (20–50 mm), and basal (50–80 mm). To check for SL deposition, sections were stained for 1 h with Fluorol Yellow 088 (Brundrett et al., 1991). Stained sections were viewed under a confocal laser scanning microscope (FV3000, Olympus) with excitation at 514 nm and detection at 520 to 550 nm and a DAPI filter (excitation at 405 nm, detection at 420–460 nm). Root images shown represent the typical results of at least six independent rice plants.

ChIP Using Arabidopsis Protoplasts

Mesophyll protoplasts were isolated from leaves of 4-week-old wild-type Arabidopsis ecotype Columbia plants and transfected according to the protocol described earlier (Yoo et al., 2007), with minor modifications. For each transfection, 8 to 15 μg of purified plasmid DNA (*35S::AtWRKY33*, *35S::AtWRKY6*, and *35S::AtWRKY9*) was used. The three WRKYs were chosen to ensure that the interaction was specific to WRKY33 (Group I WRKY) and distinct from WRKY6 and WRKY9, which also belong to Group I. A polyethylene glycol-calcium chloride transfection solution was used as follows: 25% (w/v) polyethylene glycol, 0.4 M mannitol, and 150 mM $CaCl_2$. The transfected protoplasts were incubated for 20 h at room temperature and fixed with formaldehyde. Protoplasts transfected with empty vectors were treated as the negative control. Anti-HA monoclonal antibody (Santa Cruz Biotechnology) bound to Protein-A agarose beads (Sigma) was used to immunoprecipitate the genomic DNA fragments. ChIP-qPCR analysis was carried out to check for promoter fragment enrichment in the final eluted chromatin from the ChIP experiment. Fold change in the enrichment of promoter fragments compared to the control was plotted. Results are based on data from three independent biological replicates each with at least three technical replicates.

Luciferase Assay Using Arabidopsis Protoplasts

Mesophyll protoplasts were isolated from leaves of 4-week-old *atwrky33* mutant seedlings and the luciferase assay was carried out as described earlier (Iwata et al., 2011). A sequence 1 kb upstream of *AtCYP94B1* was cloned into the pGreen II-0800-LUC vector using *Sac*I and *Xma*I restriction enzyme sites to generate the reporter. The vector with the *pAtCYP94B1* promoter (*pATCYP94B1::LUC*) was used as a reference control (reporter), while *35S::AtWRKY33* was used as the effector. Two WRKY binding sites in the *AtCYP94B1* promoter fragment were mutated (TTGAC to TTacC; Supplemental Fig. S6B) by site-directed mutagenesis, and the mutant promoter was cloned into the pGreen II-0800-LUC vector and used as an additional control. The luciferase assay was carried out using the Dual-Luciferase Reporter Assay System (Promega) according to the manufacturer's instructions. Luminescence was measured using the GloMax discover (Promega). Firefly luciferase activity was normalized to *Renilla* luciferase activity. Data shown were taken from four independent biological replicates each with three technical replicates.

Y1H Assays

Y1H assays were performed using a Matchmaker Gold Y1H System (Clontech) according to the manufacturer's instructions. The promoter fragment 2 kb upstream of *AtCYP94B1* was cloned into the pAbAi vector upstream of the *AUR1-C* reporter gene using *Sac*I and *Xma*I restriction enzyme sites. CDSs of *AtWRKY33*, *AtWRKY6*, and *AtWRKY9* were cloned separately into the pGADT7-AD vector. The primers used for cloning are listed in Supplemental Table S1. The *Saccharomyces cerevisiae* strains were then allowed to grow for 2 to 3 d at 30°C to assess DNA–protein interactions.

Statistical Analysis

Data presented are the means ± SE/SD. Binary comparisons of data were statistically analyzed by Student's *t* test ($P < 0.05$ and $P < 0.01$). For multiple comparisons between wild-type, mutant, and transgenic lines, one-way ANOVA was performed and Tukey-Kramer posthoc test was subsequently used as a multiple comparison procedure ($P < 0.05$ and $P < 0.01$).

Accession Numbers

The accession numbers of genes used in this paper are provided in Supplemental Table S2

Supplemental Data

The following supplemental materials are available.

Supplemental Figure S1. AoCYP94B1 is highly similar to other plant CYP94B subfamily members.

Supplemental Figure S2. *pAtCYP94B1::GUS* expression and growth of 4-week-old wild-type, *atcyp94b1*, and *35S::AoCYP94B1* Arabidopsis plants.

Supplemental Figure S3. Wild-type, *atcyp94b1*, *35S::AoCYP94B1*, and *AtCYP94B1::AtCYP94B1* complementation lines of Arabidopsis respond similarly to mannitol treatment.

Supplemental Figure S4. FDA penetration into endodermal cells shows functionality of suberin.

Supplemental Figure S5. Heterologous expression of *AoCYP94B1* increases deposition of an apoplastic barrier (SL) in the roots of transgenic rice seedlings.

Supplemental Figure S6. Promoter analysis of *AtCYP94B1.*

Supplemental Figure S7. *A. officinalis* WRKY33 shares high sequence similarity with Arabidopsis WRKY33.

Supplemental Figure S8. Tissue-specific expression of *pAtWRKY33::GUS.*

Supplemental Figure S9. Details of *atcyp94b1* and heterologous expression lines.

Supplemental Figure S10. Details of Arabidopsis *wrky33.*

Supplemental Table S1. Primer sequences used in the study.

Supplemental Table S2. Accession numbers used in the study.

ACKNOWLEDGMENTS

We thank the National Parks Board, Government of Singapore, for granting us permission to collect the mangrove samples from Berlayer Creek and Sungei Buloh Wetland Reserves.

Received August 10, 2020; accepted September 6, 2020; published September 14, 2020.

LITERATURE CITED

Agarwal P, Dabi M, Agarwal PK (2014) Molecular cloning and characterization of a group II WRKY transcription factor from *Jatropha curcas*, an important biofuel crop. DNA Cell Biol **33:** 503–513

Alonso JM, Stepanova AN, Leisse TJ, Kim CJ, Chen H, Shinn P, Stevenson DK, Zimmerman J, Barajas P, Cheuk R, et al (2003) Genome-wide insertional mutagenesis of *Arabidopsis thaliana*. Science **301:** 653–657

Andersen TG, Barberon M, Geldner N (2015) Suberization—the second life of an endodermal cell. Curr Opin Plant Biol **28:** 9–15

Arnon DI (1949) Copper enzymes in isolated chloroplasts. Polyphenoloxidase in *Beta vulgaris*. Plant Physiol **24:** 1–15

Aubert Y, Widemann E, Miesch L, Pinot F, Heitz T (2015) CYP94-mediated jasmonoyl-isoleucine hormone oxidation shapes jasmonate profiles and attenuates defence responses to *Botrytis cinerea* infection. J Exp Bot **66:** 3879–3892

Bai Y, Sunarti S, Kissoudis C, Visser RGF, van der Linden CG (2018) The role of tomato WRKY genes in plant responses to combined abiotic and biotic stresses. Front Plant Sci **9:** 801

Bakshi M, Oelmüller R (2014) WRKY transcription factors: Jack of many trades in plants. Plant Signal Behav **9:** e27700

Barberon M (2017) The endodermis as a checkpoint for nutrients. New Phytol **213:** 1604–1610

Barberon M, Vermeer JE, De Bellis D, Wang P, Naseer S, Andersen TG, Humbel BM, Nawrath C, Takano J, Salt DE, et al (2016) Adaptation of root function by nutrient-induced plasticity of endodermal differentiation. Cell **164:** 447–459

Benveniste I, Saito T, Wang Y, Kandel S, Huang H, Pinot FA, Kahn R, Salaun J, Shimoji M (2006) Evolutionary relationship and substrate specificity of *Arabidopsis thaliana* fatty acid omega-hydroxylase. Plant Sci **170:** 326–338

Bernards MA, Summerhurst DK, Razem FA (2004) Oxidases, peroxidases and hydrogen peroxide: The suberin connection. Phytochem Rev **3:** 113–142

Birkenbihl RP, Kracher B, Roccaro M, Somssich IE (2017) Induced genome-wide binding of three *Arabidopsis* WRKY transcription factors during early MAMP-triggered immunity. Plant Cell **29:** 20–38

Bruckhoff V, Haroth S, Feussner K, König S, Brodhun F, Feussner I (2016) Functional characterization of CYP94-genes and identification of a novel jasmonate catabolite in flowers. PLoS One **11:** e0159875

Brundrett MC, Kendrick B, Peterson CA (1991) Efficient lipid staining in plant material with Sudan red 7B or Fluorol yellow 088 in polyethylene glycol-glycerol. Biotech Histochem **66:** 111–116

Chen J, Nolan TM, Ye H, Zhang M, Tong H, Xin P, Chu J, Chu C, Li Z, Yin Y (2017) *Arabidopsis* WRKY46, WRKY54, and WRKY70 transcription factors are involved in brassinosteroid-regulated plant growth and drought responses. Plant Cell **29:** 1425–1439

Chen T, Cai X, Wu X, Karahara I, Schreiber L, Lin J (2011) Casparian strip development and its potential function in salt tolerance. Plant Signal Behav **6:** 1499–1502

Chu X, Wang C, Chen X, Lu W, Li H, Wang X, Hao L, Guo X (2015) The cotton WRKY Gene *GhWRKY41* positively regulates salt and drought stress tolerance in transgenic *Nicotiana benthamiana*. PLoS One **10:** e0143022

Clough SJ, Bent AF (1998) Floral dip: A simplified method for *Agrobacterium*-mediated transformation of *Arabidopsis thaliana*. Plant J **16:** 735–743

Cohen H, Fedyuk V, Wang C, Wu S, Aharoni A (2020) SUBERMAN regulates developmental suberization of the Arabidopsis root endodermis. Plant J **102:** 431–447

Compagnon V, Diehl P, Benveniste I, Meyer D, Schaller H, Schreiber L, Franke R, Pinot F (2009) CYP86B1 is required for very long chain ω-hydroxyacid and α,ω-dicarboxylic acid synthesis in root and seed suberin polyester. Plant Physiol **150:** 1831–1843

Dellaporta SL, Wood J, Hicks JB (1983) Plant DNA minipreparation: Version II. Plant Mol Biol Report **1:** 19–21

Enstone DE, Peterson CA, Ma FS (2003) Root endodermis and exodermis: Structure, function, and responses to the environment. J Plant Growth Regul **21:** 335–351

Franke R, Briesen I, Wojciechowski T, Faust A, Yephremov A, Nawrath C, Schreiber L (2005) Apoplastic polyesters in *Arabidopsis* surface tissues—a typical suberin and a particular cutin. Phytochemistry **66:** 2643–2658

Franke R, Höfer R, Briesen I, Emsermann M, Efremova N, Yephremov A, Schreiber L (2009) The DAISY gene from *Arabidopsis* encodes a fatty acid elongase condensing enzyme involved in the biosynthesis of aliphatic suberin in roots and the chalaza-micropyle region of seeds. Plant J **57:** 80–95

Franke R, Schreiber L (2007) Suberin—a biopolyester forming apoplastic plant interfaces. Curr Opin Plant Biol **10:** 252–259

Franke RB, Dombrink I, Schreiber L (2012) Suberin goes genomics: Use of a short living plant to investigate a long lasting polymer. Front Plant Sci **3:** 4

Gou M, Hou G, Yang H, Zhang X, Cai Y, Kai G, Liu CJ (2017) The MYB107 transcription factor positively regulates suberin biosynthesis. Plant Physiol **173:** 1045–1058

Graça J (2015) Suberin: The biopolyester at the frontier of plants. Front Chem **3:** 62

Hazman M, Sühnel M, Schäfer S, Zumsteg J, Lesot A, Beltran F, Marquis V, Herrgott L, Miesch L, Riemann M, et al (2019) Characterization of jasmonoyl-isoleucine (JA-Ile) hormonal catabolic pathways in rice upon wounding and salt stress. Rice **12:** 5

He GH, Xu JY, Wang YX, Liu JM, Li PS, Chen M, Ma YZ, Xu ZS (2016) Drought-responsive WRKY transcription factor genes *TaWRKY1* and *TaWRKY33* from wheat confer drought and/or heat resistance in *Arabidopsis*. BMC Plant Biol **16:** 116

Höfer R, Briesen I, Beck M, Pinot F, Schreiber L, Franke R (2008) The *Arabidopsis* cytochrome P450 CYP86A1 encodes a fatty acid ω-hydroxylase involved in suberin monomer biosynthesis. J Exp Bot **59:** 2347–2360

Iwata Y, Lee MH, Koizumi N (2011) Analysis of a transcription factor using transient assay in *Arabidopsis* protoplasts. *In* L Yuan, SE Perry, eds, Plant Transcription Factors, Methods in Molecular Biology **754**, Springer, New York, pp 107–117

Jiang Y, Deyholos MK (2009) Functional characterization of *Arabidopsis* NaCl-inducible WRKY25 and WRKY33 transcription factors in abiotic stresses. Plant Mol Biol **69:** 91–105

Kamiya T, Borghi M, Wang P, Danku JM, Kalmbach L, Hosmani PS, Naseer S, Fujiwara T, Geldner N, Salt DE (2015) The MYB36 transcription factor orchestrates Casparian strip formation. Proc Natl Acad Sci USA **112:** 10533–10538

Kolattukudy PE (1984) Biochemistry and function of cutin and suberin. Can J Bot **62:** 2918–2933

Koo AJ, Cooke TF, Howe GA (2011) Cytochrome P450 CYP94B3 mediates catabolism and inactivation of the plant hormone jasmonoyl-L-isoleucine. Proc Natl Acad Sci USA **108:** 9298–9303

Koo AJ, Thireault C, Zemelis S, Poudel AN, Zhang T, Kitaoka N, Brandizzi F, Matsuura H, Howe GA (2014) Endoplasmic reticulum-associated inactivation of the hormone jasmonoyl-L-isoleucine by multiple members of the cytochrome P450 94 family in *Arabidopsis*. J Biol Chem **289:** 29728–29738

Kosma DK, Murmu J, Razeq FM, Santos P, Bourgault R, Molina I, Rowland O (2014) AtMYB41 activates ectopic suberin synthesis and assembly in multiple plant species and cell types. Plant J **80:** 216–229

Kreszies T, Schreiber L, Ranathunge K (2018) Suberized transport barriers in Arabidopsis, barley and rice roots: From the model plant to crop species. J Plant Physiol **227:** 75–83

Krishnamurthy P, Jyothi-Prakash PA, Qin L, He J, Lin Q, Loh CS, Kumar PP (2014) Role of root hydrophobic barriers in salt exclusion of a mangrove plant *Avicennia officinalis*. Plant Cell Environ **37:** 1656–1671

Krishnamurthy P, Mohanty B, Wijaya E, Lee DY, Lim TM, Lin Q, Xu J, Loh CS, Kumar PP (2017) Transcriptomics analysis of salt stress tolerance in the roots of the mangrove *Avicennia officinalis*. Sci Rep **7:** 10031

Krishnamurthy P, Ranathunge K, Franke R, Prakash HS, Schreiber L, Mathew MK (2009) The role of root apoplastic transport barriers in salt tolerance of rice (*Oryza sativa* L.). Planta **230:** 119–134

Krishnamurthy P, Ranathunge K, Nayak S, Schreiber L, Mathew MK (2011) Root apoplastic barriers block Na^+ transport to shoots in rice (*Oryza sativa* L.). J Exp Bot **62:** 4215–4228

Kronzucker HJ, Britto DT (2011) Sodium transport in plants: A critical review. New Phytol **189:** 54–81

Kurotani K, Hayashi K, Hatanaka S, Toda Y, Ogawa D, Ichikawa H, Ishimaru Y, Tashita R, Suzuki T, Ueda M, et al (2015) Elevated levels of CYP94 family gene expression alleviate the jasmonate response and enhance salt tolerance in rice. Plant Cell Physiol **56:** 779–789

Li P, Yu Q, Gu X, Xu C, Qi S, Wang H, Zhong F, Baskin TI, Rahman A, Wu S (2018) Construction of a functional Casparian strip in non-endodermal lineages is orchestrated by two parallel signaling systems in *Arabidopsis thaliana*. Curr Biol **28:** 2777–2786

Liang QY, Wu YH, Wang K, Bai ZY, Liu QL, Pan YZ, Zhang L, Jiang BB (2017) Chrysanthemum WRKY gene *DgWRKY5* enhances tolerance to salt stress in transgenic chrysanthemum. Sci Rep **7:** 4799

Lunde C, Kimberlin A, Leiboff S, Koo AJ, Hake S (2019) *Tasselseed5* overexpresses a wound-inducible enzyme, *ZmCYP94B1*, that affects jasmonate catabolism, sex determination, and plant architecture in maize. Commun Biol **2:** 114

Ma FS, Peterson CA (2003) Current insights into the development, structure and chemistry of the endodermis and exodermis of roots. Can J Bot **81:** 405–421

Mahalingam R, Gomez-Buitrago A, Eckardt N, Shah N, Guevara-Garcia A, Day P, Raina R, Fedoroff NV (2003) Characterizing the stress/defense transcriptome of Arabidopsis. Genome Biol **4:** R20

Narusaka Y, Narusaka M, Seki M, Umezawa T, Ishida J, Nakajima M, Enju A, Shinozaki K (2004) Crosstalk in the responses to abiotic and

biotic stresses in *Arabidopsis*: Analysis of gene expression in cytochrome P450 gene superfamily by cDNA microarray. Plant Mol Biol **55:** 327–342

Naseer S, Lee Y, Lapierre C, Franke R, Nawrath C, Geldner N (2012) Casparian strip diffusion barrier in *Arabidopsis* is made of a lignin polymer without suberin. Proc Natl Acad Sci USA **109:** 10101–10106

Nawrath C, Schreiber L, Franke RB, Geldner N, Reina-Pinto JJ, Kunst L (2013) Apoplastic diffusion barriers in Arabidopsis. In The Arabdiopsis Book, Vol **11**. p e0167

Okay S, Derelli E, Unver T (2014) Transcriptome-wide identification of bread wheat WRKY transcription factors in response to drought stress. Mol Genet Genomics **289:** 765–781

Parida AK, Das AB (2005) Salt tolerance and salinity effects on plants: A review. Ecotoxicol Environ Saf **60:** 324–349

Pinot F, Beisson F (2011) Cytochrome P450 metabolizing fatty acids in plants: Characterization and physiological roles. FEBS J **278:** 195–205

Ranathunge K, Lin J, Steudle E, Schreiber L (2011a) Stagnant deoxygenated growth enhances root suberization and lignifications, but differentially affects water and NaCl permeabilities in rice (*Oryza sativa* L.) roots. Plant Cell Environ **34:** 1223–1240

Ranathunge K, Schreiber L (2011) Water and solute permeabilities of *Arabidopsis* roots in relation to the amount and composition of aliphatic suberin. J Exp Bot **62:** 1961–1974

Ranathunge K, Schreiber L, Franke R (2011b) Suberin research in the genomics era—new interest for an old polymer. Plant Sci **180:** 399–413

Ranathunge K, Steudle E, Lafitte R (2005) Blockage of apoplastic bypass-flow of water in rice roots by insoluble salt precipitates analogous to a Pfeffer cell. Plant Cell Environ **28:** 121–133

Ranathunge K, Thomas RH, Fang X, Peterson CA, Gijzen M, Bernards MA (2008) Soybean root suberin and partial resistance to root rot caused by *Phytophthora sojae*. Phytopathology **98:** 1179–1189

Sarris PF, Duxbury Z, Huh SU, Ma Y, Segonzac C, Sklenar J, Derbyshire P, Cevik V, Rallapalli G, Saucet SB, et al (2015) A plant immune receptor detects pathogen effectors that target WRKY transcription factors. Cell **161:** 1089–1100

Scholander PF (1968) How mangroves desalinate water. Physiol Plant **21:** 251–261

Schreiber L, Franke BR (2011) Endodermis and exodermis in roots. eLS, doi: 10.1002/9780470015902.a0002086.pub2

Schreiber L, Hartmann K, Skrabs M, Zeier J (1999) Apoplastic barriers in roots: Chemical composition of endodermal and hypodermal cell walls. J Exp Bot **50:** 1267–1280

Song H, Wang P, Hou L, Zhao S, Zhao C, Xia H, Li P, Zhang Y, Bian X, Wang X (2016) Global analysis of WRKY genes and their response to dehydration and salt stress in soybean. Front Plant Sci **7:** 9

Toki S, Hara N, Ono K, Onodera H, Tagiri A, Oka S, Tanaka H (2006) Early infection of scutellum tissue with *Agrobacterium* allows high-speed transformation of rice. Plant J **47:** 969–976

Ursache R, Andersen TG, Marhavý P, Geldner N (2018) A protocol for combining fluorescent proteins with histological stains for diverse cell wall components. Plant J **93:** 399–412

Widemann E, Smirnova E, Aubert Y, Miesch L, Heitz T (2016) Dynamics of jasmonate metabolism upon flowering and across leaf stress responses in *Arabidopsis thaliana*. Plants (Basel) **5:** 1–15

Wu M, Liu H, Han G, Cai R, Pan F, Xiang Y (2017) A moso bamboo WRKY gene *PeWRKY83* confers salinity tolerance in transgenic *Arabidopsis* plants. Sci Rep **7:** 11721

Wunderling A, Ripper D, Barra-Jimenez A, Mahn S, Sajak K, Targem MB, Ragni L (2018) A molecular framework to study periderm formation in Arabidopsis. New Phytol **219:** 216–229

Xu YH, Wang JW, Wang S, Wang JY, Chen XY (2004) Characterization of GaWRKY1, a cotton transcription factor that regulates the sesquiterpene synthase gene (+)-δ-cadinene synthase-A. Plant Physiol **135:** 507–515

Yeo AR, Yeo ME, Flowers TJ (1987) The contribution of an apoplastic pathway to sodium uptake by rice roots in saline conditions. J Exp Bot **38:** 1141–1153

Yoo SD, Cho YH, Sheen J (2007) Arabidopsis mesophyll protoplasts: A versatile cell system for transient gene expression analysis. Nat Protoc **2:** 1565–1572

Yoshida S, Forno DA, Cock JH (1971) Laboratory Manual for Physiological Studies of Rice. Internation Rice Research Institute, Los Baños, Philippines, pp 1–83